



HAL
open science

Escherichia coli Rho GTPase-activating toxin CNF1 mediates NLRP3 inflammasome activation via p21-activated kinases-1/2 during bacteraemia in mice

Océane Dufies, Anne Doye, Johan Courjon, Cédric Torre, Gregory Michel, Celine Loubatier, Arnaud Jacquél, Paul Chaintreuil, Alissa Majoor, Rodolphe r. Guinamard, et al.

► To cite this version:

Océane Dufies, Anne Doye, Johan Courjon, Cédric Torre, Gregory Michel, et al.. Escherichia coli Rho GTPase-activating toxin CNF1 mediates NLRP3 inflammasome activation via p21-activated kinases-1/2 during bacteraemia in mice. *Nature Microbiology*, 2021, 6 (3), pp.401 - 412. 10.1038/s41564-020-00832-5 . hal-03473187

HAL Id: hal-03473187

<https://hal.science/hal-03473187>

Submitted on 9 Dec 2021

HAL is a multi-disciplinary open access archive for the deposit and dissemination of scientific research documents, whether they are published or not. The documents may come from teaching and research institutions in France or abroad, or from public or private research centers.

L'archive ouverte pluridisciplinaire **HAL**, est destinée au dépôt et à la diffusion de documents scientifiques de niveau recherche, publiés ou non, émanant des établissements d'enseignement et de recherche français ou étrangers, des laboratoires publics ou privés.



Escherichia coli Rho GTPase-activating toxin CNF1 mediates NLRP3 inflammasome activation via p21-activated kinases-1/2 during bacteraemia in mice

Océane Dufies¹, Anne Doye¹, Johan Courjon^{1,2}, Cédric Torre¹, Gregory Michel¹, Celine Loubatier¹, Arnaud Jacquet¹, Paul Chaintreuil¹, Alissa Major¹, Rodolphe R. Guinamard¹, Alexandre Gallerand¹, Pedro H. V. Saavedra³, Els Verhoeven^{1,4}, Amaury Rey^{1,4}, Sandrine Marchetti¹, Raymond Ruimy^{1,2}, Dorota Czerucka^{5,6}, Mohamed Lamkanfi³, Bénédicte F. Py⁴, Patrick Munro¹, Orane Visvikis¹ and Laurent Boyer^{1,6} ✉

Inflammasomes are signalling platforms that are assembled in response to infection or sterile inflammation by cytosolic pattern recognition receptors. The consequent inflammasome-triggered caspase-1 activation is critical for the host defence against pathogens. During infection, NLRP3, which is a pattern recognition receptor that is also known as cryopyrin, triggers the assembly of the inflammasome-activating caspase-1 through the recruitment of ASC and Nek7. The activation of the NLRP3 inflammasome is tightly controlled both transcriptionally and post-translationally. Despite the importance of the NLRP3 inflammasome regulation in autoinflammatory and infectious diseases, little is known about the mechanism controlling the activation of NLRP3 and the upstream signalling that regulates the NLRP3 inflammasome assembly. We have previously shown that the Rho-GTPase-activating toxin from *Escherichia coli* cytotoxic necrotizing factor-1 (CNF1) activates caspase-1, but the upstream mechanism is unclear. Here, we provide evidence of the role of the NLRP3 inflammasome in sensing the activity of bacterial toxins and virulence factors that activate host Rho GTPases. We demonstrate that this activation relies on the monitoring of the toxin's activity on the Rho GTPase Rac2. We also show that the NLRP3 inflammasome is activated by a signalling cascade that involves the p21-activated kinases 1 and 2 (Pak1/2) and the Pak1-mediated phosphorylation of Thr 659 of NLRP3, which is necessary for the NLRP3-Nek7 interaction, inflammasome activation and IL-1 β cytokine maturation. Furthermore, inhibition of the Pak-NLRP3 axis decreases the bacterial clearance of CNF1-expressing UTI89 *E. coli* during bacteraemia in mice. Taken together, our results establish that Pak1 and Pak2 are critical regulators of the NLRP3 inflammasome and reveal the role of the Pak-NLRP3 signalling axis in vivo during bacteraemia in mice.

Uropathogenic *E. coli* is the leading causative agent of bacteraemia¹. It is therefore fundamental to decipher the mechanisms that determine the fate of this pathogen in the blood. The innate immune sensing of *E. coli* is mediated by pattern recognition receptors (PRRs), mainly by Toll-like receptor-4 (TLR4), which detects bacterial lipopolysaccharides (LPS). LPS are the principal component of the external membrane of both pathogenic and non-pathogenic *E. coli* and, therefore, pattern-triggered immunity does not seem to be sufficient to gauge the pathogenic potential of microorganisms. As TLR4 is activated by both live and dead bacteria, pattern-triggered immunity is certainly important for monitoring the quantity of bacteria, but is not sufficient to determine their quality². One strategy to determine microbial pathogenicity is the detection of virulence factor activities that are specific to pathogens³. Virulence factors of uropathogenic *E. coli* include CNF1, which is a Rho-GTPase-targeting toxin. The CNF1 toxin bears enzymatic activity that is responsible for the post-translational deamidation

of a specific glutamine residue on a subset of Rho GTPases, namely Rac, Cdc42 and RhoA^{4–6}. This modification destroys the intrinsic and GTPase-activating-protein- (GAP)-regulated ability of these Rho GTPases to hydrolyse GTP, conferring dominant positive mutant characteristics to Rho proteins^{4–6}. This modification increases GTP-bound activated Rho proteins and the activation of their downstream signalling pathways⁶. By modulating the host cytoskeleton, these virulence factors confer to bacteria invasion properties and the ability to modulate inflammatory responses^{7–10}. Among the virulence factors, there are more than 30 that target Rho GTPases. They are either activators or inhibitors of Rho GTPases, both of which activate caspase-1 (refs. ^{11,12}).

Inflammasomes are signalling platforms that are assembled by cytosolic PRRs that activate caspase-1. NLRP3 oligomerizes on infection or cellular damage, and recruits ASC, Nek7 and caspase-1 to form the NLRP3 inflammasome. This assembly results in ASC speck formation, cleavage of pro-caspase-1 into active caspase-1 and

¹Université Côte d'Azur, Inserm, C3M, Nice, France. ²Université Côte d'Azur, CHU Nice, Nice, France. ³Department of Internal Medicine and Pediatrics, Ghent University, Ghent, Belgium. ⁴CIRI, Centre International de Recherche en Infectiologie, Université de Lyon, Inserm U1111, Université Claude Bernard Lyon 1, CNRS UMR5308, ENS de Lyon, Lyon, France. ⁵Centre Scientifique de Monaco, Monaco, Monaco. ⁶LIA ROPSE, Laboratoire International Associé Université Côte d'Azur, Centre Scientifique de Monaco, Nice, France. ✉e-mail: laurent.boyer@univ-cotedazur.fr

the maturation of pro-IL-1 β into IL-1 β . The NLRP3 inflammasome assembly is controlled by both the priming by TLR ligands and activation signals. Furthermore, the NLRP3 inflammasome assembly is regulated by phosphorylation and ubiquitination events^{13,14}. Despite a variety of identified NLRP3 activators, the upstream signalling pathways that control NLRP3 post-translational modifications and activation mechanisms remain unclear¹⁴. Interestingly, toxins that inactivate Rho GTPases activate the Pyrin inflammasome through the modification of its phosphorylation status by the PKN1/2 kinases. The Pyrin inflammasome has been shown to detect toxins that inhibit Rho GTPases, but information about the sensing of toxins that activate Rho GTPases through inflammasomes is lacking^{15,16}. In this Article, we used the CNF1 toxin as a model of the Rho-GTPase-activating virulence factor to demonstrate the role of the Pak–NLRP3 axis in sensing CNF1 activity and controlling the clearance of bacteria during bacteraemia.

Results

CNF1-triggered immunity requires NLRP3. We set up an assay to monitor the CNF1-triggered activation of caspase-1 using a FAM-YVAD-FMK (FAM-FLICA) probe. Primary bone-marrow-derived macrophages (BMDMs) isolated from BALB/c mice were treated with CNF1 and analysed using confocal microscopy. Cells with dots of FAM-FLICA staining corresponding to ASC specks were counted (Extended Data Fig. 1a). This unbiased screen revealed that NLRP3 is the major NLR involved in CNF1-triggered caspase-1 activation (Fig. 1a). The role of NLRP3 in this pathway was confirmed in BMDMs isolated from C57BL/6J mice bearing ASC–citricine knockin using flow cytometry (Extended Data Fig. 1b,c). In this assay, we quantified the percentage of cells with ASC specks as previously described^{17,18}. These data revealed the conserved role of NLRP3 in the response to CNF1 in macrophages isolated from both BALB/c and C57BL/6J background.

Next, we investigated the role of NLRP3 in CNF1-triggered immunity. Co-treatment of BMDMs isolated from wild-type (WT) mice with the CNF1 toxin together with the NLRP3 inhibitor MCC950 was sufficient to block caspase-1 activity, demonstrating that the CNF1 toxin is an NLRP3 activator (Fig. 1b,c). Importantly, the number of FAM-FLICA⁺ cells was substantially reduced in BMDMs that were treated with catalytically inactive mutant CNF1^{C866S}. This result provided evidence that CNF1 toxin activity is monitored by NLRP3, rather than the pattern of the toxin³. Furthermore, CNF1-triggered maturation and secretion of IL-1 β and activation of caspase-1 was impaired in NLRP3-knockout BMDMs (Fig. 1d and Supplementary Fig. 1). By contrast, CNF1 treatment did not affect the secretion of IL-6 or TNF- α , two cytokines that are not regulated by inflammasomes (Fig. 1d and Supplementary Fig. 1). Activation of the NLRP3 inflammasome is often associated with pyroptosis¹⁹. To investigate whether CNF1 triggered pyroptosis, we measured propidium iodide incorporation (Extended Data Fig. 2a), lactate dehydrogenase (LDH) release (Extended Data Fig. 2b) and gasdermin D (GSDMD) cleavage (Extended Data Fig. 2c). In contrast to nigericin, we did not observe any of these pyroptosis markers after CNF1 treatment and we observed a similar level of CNF1-triggered caspase-1 activation and IL-1 β maturation/secretion in WT and GSDMD-knockout macrophages (Extended Data Fig. 2d,e). We subsequently tested the role of the NLRP3 inflammasome regulator Nek7 in CNF1-triggered immunity. Transfection of *Nlrp3* or *Nek7* short interfering RNA (siRNA) in BMDMs inhibited CNF1-triggered IL-1 β maturation (Extended Data Fig. 3a,b). K⁺ efflux is an upstream event for NLRP3 inflammasome activation and Nek7 requires K⁺ efflux for NLRP3 inflammasome assembly^{14,20}. We observed that KCl treatment was sufficient to inhibit CNF1-triggered caspase-1 cleavage (Extended Data Fig. 3c). Importantly, we confirmed that the KCl treatment did not inhibit CNF1 toxin activity towards Rho GTPase activation using a glutathione S-transferase (GST)–Pak–Rac-binding domain

(RBD) pull-down assay (Extended Data Fig. 3d). We next investigated whether other toxins that target Rho GTPases have the ability to activate the NLRP3 inflammasome. Dermonecrotic toxin (DNT) from *Bordetella* has transglutaminase activity towards Rho GTPases that enables the constitutive activation of Rho GTPases^{6,10}. We observed that purified recombinant DNT triggered the activation of caspase-1 in WT macrophages, but not in NLRP3-knockout macrophages (Extended Data Fig. 4a). We next tested whether the NLRP3 activation was triggered specifically by virulence factors activating Rho GTPases using NLRP3 inflammasome reconstitution in HEK293T cells²¹. Cells were transfected with plasmids encoding the DNT toxin or the injected bacterial virulence factors YopE from *Yersinia* containing a GAP domain that enables inactivation of the Rho GTPases⁶. We observed NLRP3-dependent IL-1 β maturation when cells were transfected with the Rho-GTPase-activating toxin DNT, but not when cells were transfected with the Rho GTPase inhibitor YopE (Extended Data Fig. 4b). The expression of the virulence factor SopE from *Salmonella* containing a guanine nucleotide exchange factor (GEF) domain activating Rac and Cdc42 (refs. 6,22) or the expression of the GEF domain of the Dbl exchange factor (Dbl^{495–826})²³ were sufficient to trigger NLRP3-dependent IL-1 β maturation (Extended Data Fig. 4b,c). Taken together, we showed that the activation of Rho GTPases by toxins and virulence factors triggered the activation of the NLRP3 inflammasome and that Rac has a major role in this pathway.

Activation of the NLRP3 inflammasome by CNF1 relies on Rac2 and the Pak serine–threonine kinases. Although the CNF1 toxin is a Rho GTPases activator and Rac2 is a haematopoietic-specific Rho GTPase that is involved in the innate immune response to the CNF1 toxin²⁴, the contribution of Rac1 and Rac2 in this process is still unknown. To investigate the role of Rac in the CNF1-triggered NLRP3 inflammasome activation, we knocked down *Rac1* and/or *Rac2* using siRNA in BMDMs. Interestingly, *Rac1* knockdown resulted in an increase in the level of CNF1-triggered IL-1 β maturation whereas *Rac2* knockdown was sufficient to block it (Fig. 2a). We tested whether activated GTP-bound Rac2 levels would increase when *Rac1* was targeted by siRNA. The GST–Pak–RBD pull-down analysis showed an increase in activated Rac2 when *Rac1* was knocked-down using siRNA (Fig. 2b). These data demonstrate the critical role of Rac2 in CNF1-triggered IL-1 β maturation (Fig. 2a,b). To determine the molecular mechanism of the caspase-1 activation, we used a system of NLRP3 inflammasome reconstitution in HEK293T cells. This analysis showed that CNF1 is sufficient for the NLRP3 inflammasome activation-triggered caspase-1 cleavage and that the co-treatment of CNF1 with MCC950 inhibited this caspase-1 activation (Fig. 2c). The transfection of Rac2 GTPase or activated mutant forms of Rac2 (including Q61E mimicking the CNF1 modification or Q61L and G12V) were sufficient to activate caspase-1, in contrast to the inactive mutant Rac2^{T17N} (Fig. 2d). Interestingly, the strength of caspase-1 activation observed using the activated forms of Rac2 GTPase was correlated with the amount of Rho GTPases that were bound to GST–Pak–RBD (Fig. 2e). These data indicate that NLRP3 senses the activation level of the Rho GTPase Rac2 proportionally to the strength of activation rather than by detecting the structural modification made by the toxin as it would be predicted for a classical PRR.

The correlation between caspase-1 activation and the amount of Rac2 bound to GST–Pak–RBD suggested a potential role of Pak kinases in CNF1-triggered NLRP3 inflammasome activation. We therefore knocked-down Pak1 and/or Pak2 in BMDMs by transfecting siRNA (Pak3 is predominantly expressed in the brain^{25,26}). We observed a major decrease in caspase-1 cleavage in cells treated with *Pak1* siRNA but a moderate impact when using siRNA targeting *Pak2*, indicating that Pak1 has a main role (Fig. 3a). However, we could not exclude the possibility that the total inhibition of

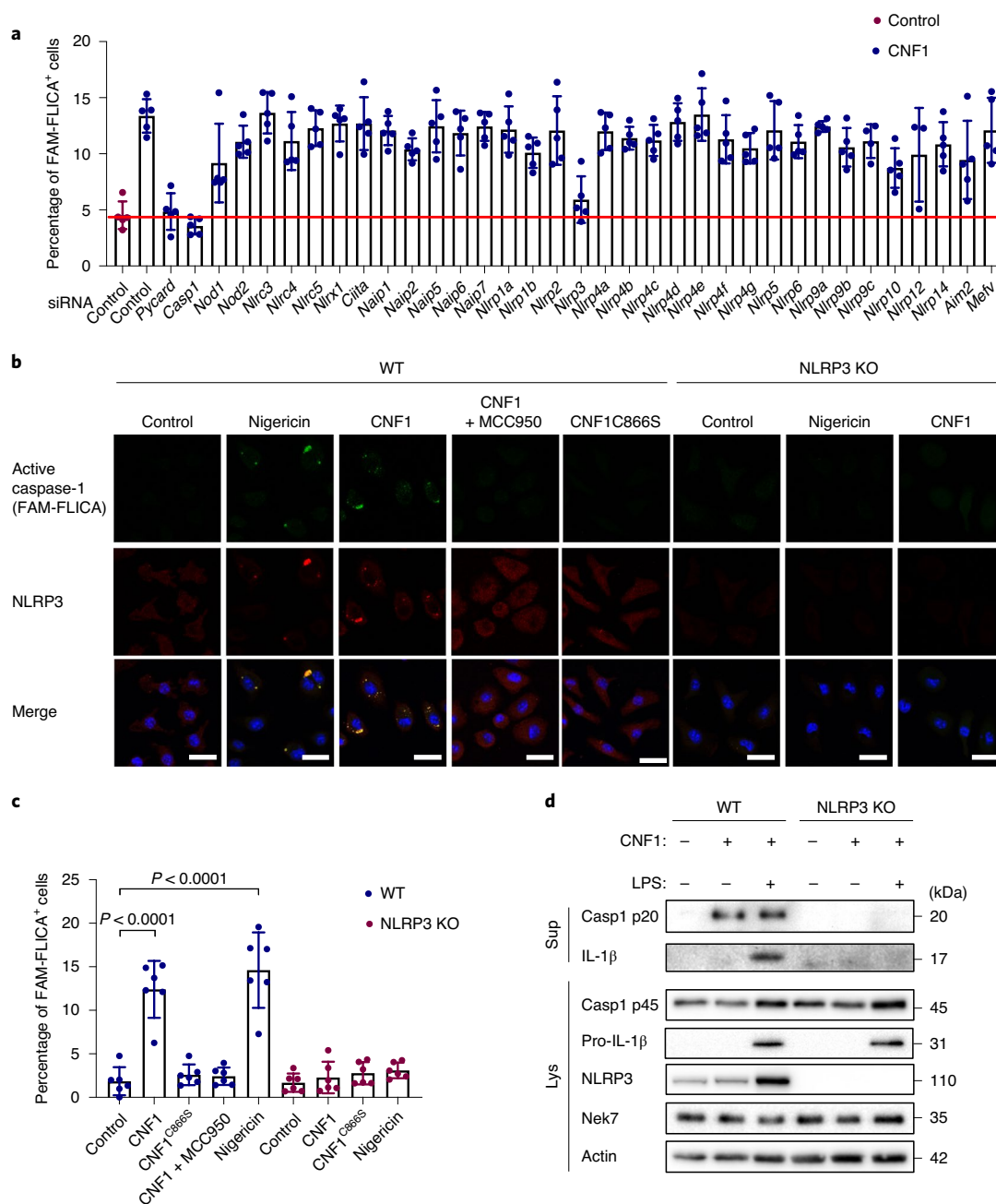


Fig. 1 | CNF1-triggered caspase-1 activation and IL-1 β maturation requires NLRP3. **a**, BMDMs isolated from BALB/c mice were transfected with the indicated siRNA for 72 h before treatment for 6 h with CNF1 (500 ng ml⁻¹). Active caspase-1 was detected using the FAM-FLICA probe. Cells harbouring FAM-FLICA dots were counted as positive using Fiji. The red horizontal line indicates the mean percentage of FAM-FLICA⁺ cells in the untreated control. Each dot represents 200 cells. $n = 1,800$ cells. Data are mean \pm s.e.m. **b, c**, BMDMs extracted from WT or NLRP3-knockout C57BL/6J mice were or were not pretreated for 45 min with MCC950 (1 μ M) before treatment for 6 h with CNF1 (500 ng ml⁻¹), or the CNF1 catalytic inactive mutant CNF1^{C866S} (500 ng ml⁻¹) or nigericin (5 μ M). **b**, Cells were analysed using immunofluorescence and confocal imaging. Active caspase-1 (FAM-FLICA) is shown in green, NLRP3 in red and nuclei in blue. Scale bars, 20 μ m. **c**, Quantification of FAM-FLICA⁺ cells in WT (blue) or NLRP3-knockout BMDMs (red). Each dot represents 100 cells. $n = 600$ cells. Data are mean \pm s.e.m. Statistical analyses were performed using two-tailed unpaired Student's *t*-tests. **d**, WT or NLRP3-knockout BMDMs were treated with CNF1 (500 ng ml⁻¹) and/or LPS (100 ng ml⁻¹) for 8 h before the supernatants (Sup) and cell lysates (Lys) were collected and analysed using immunoblotting. Experiments were repeated at least three times, and representative data are shown.

caspase-1 cleavage observed with the *Pak1* siRNA treatment might be due to a limit in the detection level of cleaved caspase-1, or to *Pak1* siRNA that may affect *Pak2*, suggesting that there is a partial *Pak1/2* redundancy. The treatment with *Pak1* inhibitors (IPA-3 or FRAX597) was sufficient to block the CNF1-triggered IL-1 β maturation that was observed in macrophages treated with LPS,

and was also sufficient to block caspase-1 activation (Fig. 3b,c). The inhibition of the caspase-1 cleavage after IPA-3 treatment was similarly observed in macrophages treated with DNT (Extended Data Fig. 4d). Interestingly, IPA-3 was shown to inhibit the binding of activated forms of Rac and Cdc42 to *Pak1*, thereby inhibiting the autophosphorylation of Thr423, whereas the FRAX597

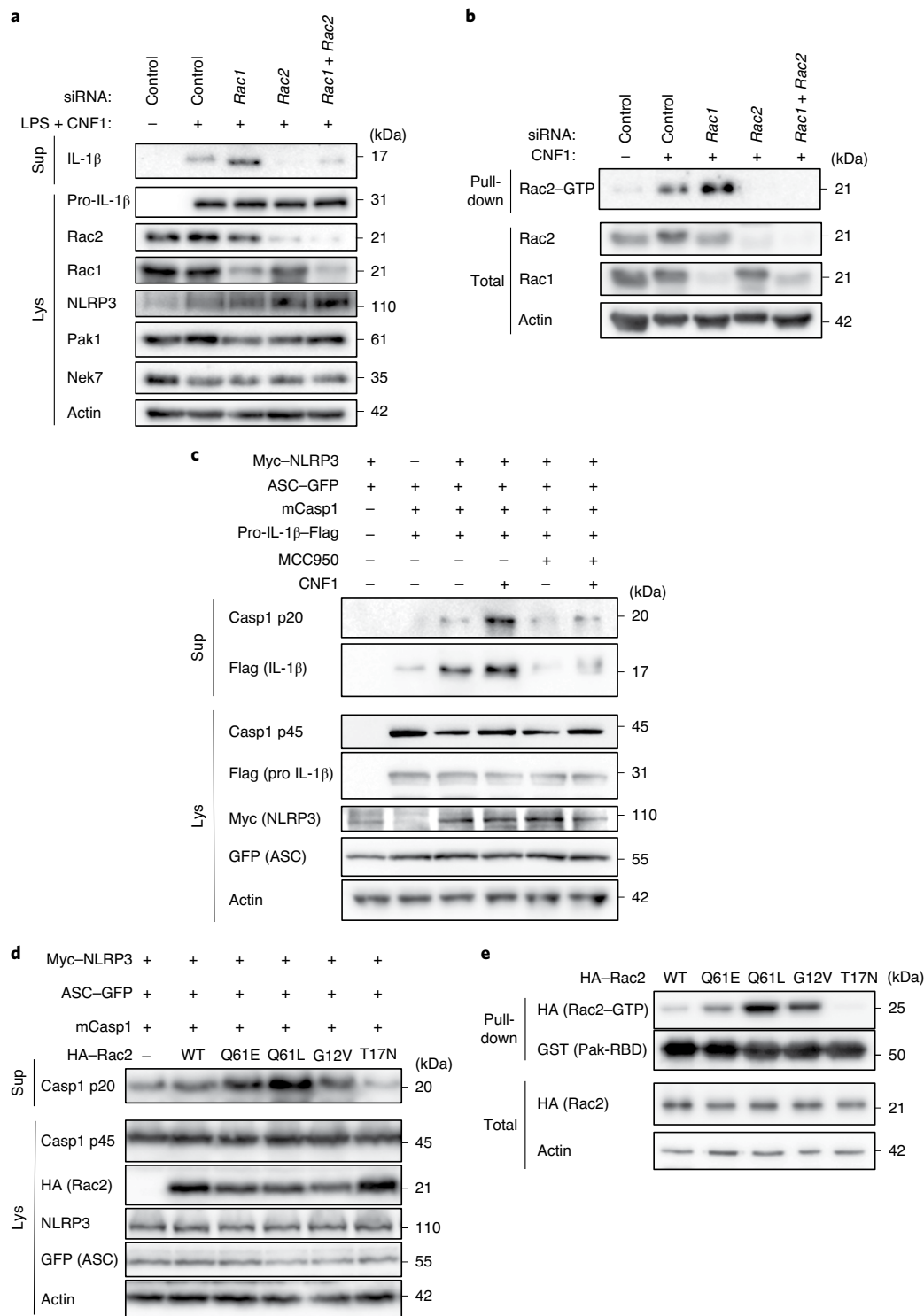


Fig. 2 | Rac2 activation triggers NLRP3 inflammasome activation. a, BMDMs extracted from BALB/c mice were transfected with siRNA targeting the indicated isoform of Rac GTPase for 72 h and treated with CNF1 (500 ng ml⁻¹) and LPS (100 ng ml⁻¹) for 8 h. Supernatants and cell lysates were analysed using immunoblotting. **b**, Immortalized BMDMs (iBMDMs) were transfected with the indicated siRNA for 72 h before being treated or not treated with CNF1 (500 ng ml⁻¹) for 6 h before analysis using a GST-Pak-RBD pull-down assay. The Rac2 associated with the GST-Pak-RBD beads is indicated as Rac2-GTP. **c,d**, HEK293T cells were transfected for 16 h with plasmids encoding NLRP3 inflammasome components: Myc-NLRP3, green fluorescent protein (GFP)-tagged ASC, mouse caspase-1 (mCasp1) and pro-IL-1 β -Flag as indicated, before analysing caspase-1 cleavage or pro-IL-1 β maturation using immunoblotting. **c**, Cells were pretreated or not with 1 μ M MCC950 for 45 min before treatment for 6 h with CNF1 (500 ng ml⁻¹). **d**, Cells were transfected with the following haemagglutinin (HA)-tagged mutants of Rac2: the constitutively active mutant mimicking CNF1-induced deamidation Rac2^{Q61E} (Q61E), the constitutively active mutants Rac2^{Q61L} (Q61L) or Rac2^{G12V} (G12V), or the dominant negative mutant Rac2^{T17N} (T17N). Supernatants and cell lysates were analysed using immunoblotting. **e**, HEK293T cells were transfected for 16 h with HA-tagged active mutants Rac2^{Q61E}, Rac2^{Q61L} or Rac2^{G12V}, or the dominant negative mutant Rac2^{T17N} before analysis using a GST-Pak-RBD pull-down assay. HA-Rac2 associated with the GST-Pak-RBD beads is indicated as Rac2-GTP. Experiments were repeated at least three times, and representative data are shown.

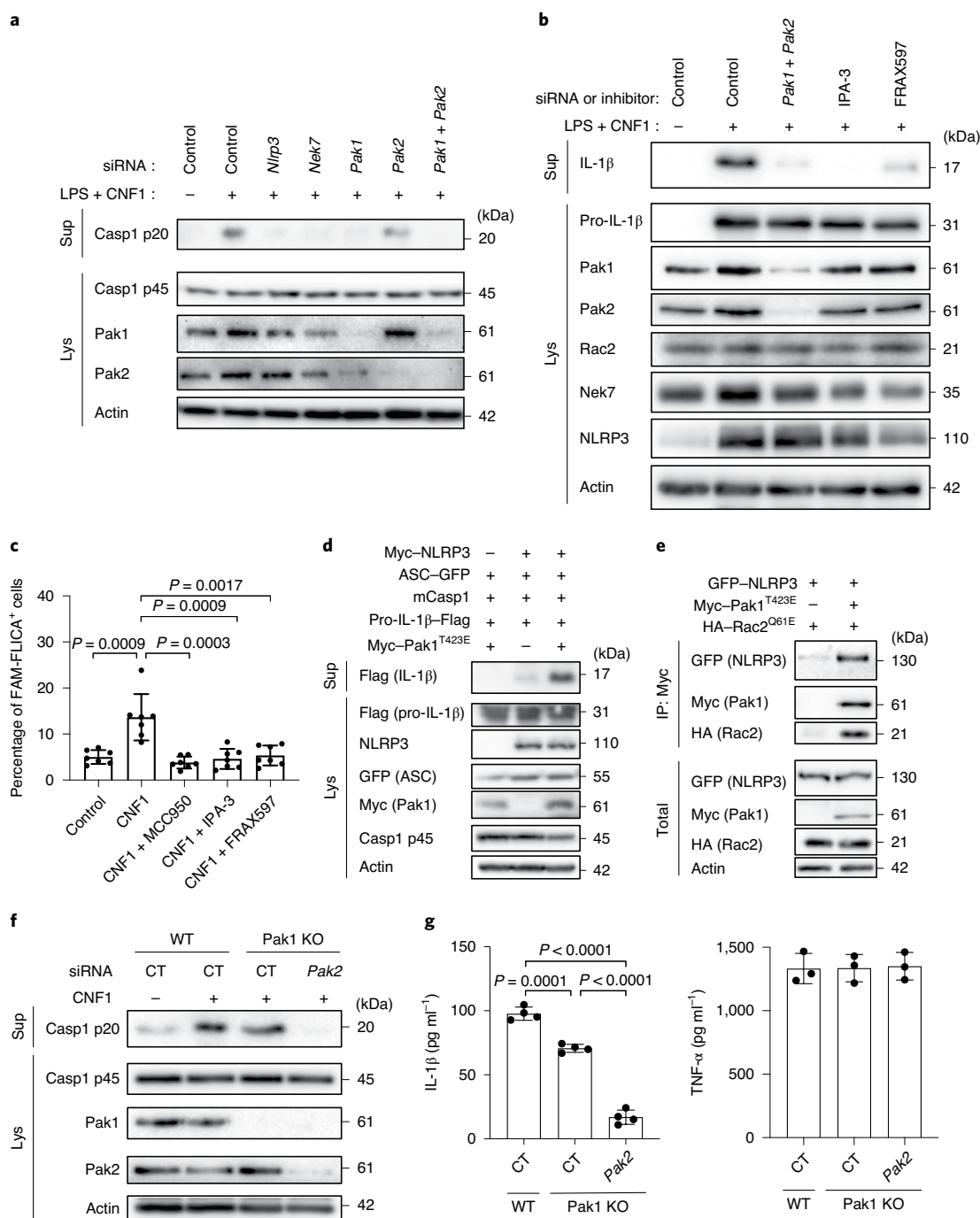


Fig. 3 | Rac2-NLRP3 signalling is dependent on Pak1 kinase. a, BMDMs isolated from BALB/c mice were transfected for 72 h with siRNA targeting *Nlrp3*, *Nek7*, *Pak1* or *Pak2* as indicated; non-targeting siRNA was used as a control. Cells were treated with CNF1 (500 ng ml⁻¹) and LPS (100 ng ml⁻¹) for 8 h, as indicated. Supernatants and cell lysates were analysed using immunoblotting. **b**, BMDMs isolated from BALB/c mice were transfected with *Pak1*- and *Pak2*-targeting siRNA or with non-targeting siRNA for 72 h, and treated with 5 μM IPA-3, 1 μM FRAX597 or vehicle for 45 min before treatment with CNF1 (500 ng ml⁻¹) and LPS (100 ng ml⁻¹) for 8 h. Supernatants and cell lysates were analysed using immunoblotting. **c**, BMDMs isolated from BALB/c mice were treated with vehicle (control), or treated either with 1 μM MCC950, 5 μM IPA-3 or 1 μM FRAX597 for 45 min before treatment with CNF1 (500 ng ml⁻¹) for 6 h. Active caspase-1 was stained with FAM-FLICA, analysed using microscopy and FAM-FLICA⁺ cells were counted. Each dot represents 100 cells. *n* = 800 cells. Data are mean ± s.e.m. Statistical analyses were performed using two-tailed unpaired Student's *t*-tests. **d**, HEK293T cells were transfected as indicated with plasmids encoding components of the NLRP3 inflammasome (Myc-NLRP3, ASC-GFP, mouse caspase-1) and pro-IL-1β-Flag together with Myc-Pak1^{T423E}, and pro-IL-1β-Flag cleavage was analysed using immunoblotting. **e**, HEK293T cells were transfected with plasmids encoding GFP-NLRP3, Myc-Pak1^{T423E} and HA-Rac2^{Q61E}. Cell lysates were processed for anti-Myc immunoprecipitation (IP). **f**, BMDMs isolated from WT or Pak1-knockout C57BL/6J mice were transfected 72 h with non-targeting or *Pak2*-targeting siRNA before treatment with CNF1 (500 ng ml⁻¹) for 8 h. Supernatants and cell lysates were analysed using immunoblotting. CT, control. **g**, BMDMs isolated from WT or Pak1-knockout C57BL/6J mice were transfected for 72 h with non-targeting or *Pak2*-targeting siRNA before treatment with CNF1 (500 ng ml⁻¹) and LPS (100 ng ml⁻¹) for 8 h. Supernatants were analysed using enzyme-linked immunosorbent assay (ELISA) for IL-1β (*n* = 4 biologically independent samples) and TNF-α (*n* = 3 biologically independent samples). Data are mean ± s.e.m. Statistical analyses were performed using two-tailed unpaired Student's *t*-tests. Experiments were repeated at least three times, and representative data are shown.

is an ATP-competitive inhibitor²⁷. In the inflammasome reconstitution system in HEK293T, we expressed the activated form of Pak1 (T423E) together with caspase-1, ASC and pro-IL-1 β , and we observed no IL-1 β maturation. By contrast, when NLRP3 was transfected together with ASC and caspase-1, the expression of the activated form of Pak1 was sufficient to trigger maturation of IL-1 β (Fig. 3d). Furthermore, phosphorylated forms of Pak colocalized in dot-like structures with NLRP3 and active caspase-1 (Supplementary Fig. 2). We next investigated whether Rac2, Pak1 and NLRP3 proteins formed a complex. We found NLRP3 interacting with activated Rac2 when activated Pak1 was expressed (Fig. 3e). We next investigated whether Pak1 was involved in the nigericin-triggered activation of the NLRP3 inflammasome and observed that IPA-3 treatment was sufficient to inhibit both caspase-1 cleavage and the release of LDH (Extended Data Fig. 5a,b). Furthermore, siRNA targeting of *Pak1* was found to decrease nigericin-triggered caspase-1 maturation (Extended Data Fig. 5c).

To genetically prove the involvement of Pak1 in NLRP3 inflammasome activation, we used Pak1-knockout mice. We observed a reduction in caspase-1 cleavage triggered by CNF1 in Pak1-knockout macrophages and a reduction in IL-1 β secretion (Fig. 3f,g). By contrast, the secretion of TNF- α was unaffected (Fig. 3g). Both caspase-1 cleavage and IL-1 β secretion triggered by CNF1 were substantially reduced when the Pak1-knockout macrophages were treated with the *Pak2* siRNA, suggesting that there is a partial compensation in Pak1-knockout macrophages (Fig. 3f,g).

Pak1 phosphorylates NLRP3 and triggers inflammasome activation. To further investigate whether NLRP3 is a substrate for the Pak1 serine–threonine kinase, we set-up an in vitro kinase assay. When both Pak1 and NLRP3 proteins were incubated with ATP- γ -³²P, we observed a band at the size of NLRP3, indicating that NLRP3 is directly phosphorylated by Pak1 in vitro (Fig. 4a). The in vitro kinase assay was then used to identify the phosphorylated sites of NLRP3 by analysing the band corresponding to NLRP3 using mass spectrometry. The analysis revealed that Pak1 phosphorylates NLRP3 at three independent positions that correspond to Ser 163, Ser 198 and Thr 659 in the human NLRP3 (Extended Data Fig. 6a,c and Supplementary Table 1). Interestingly, the Ser 163 and Ser 198 residues were previously reported to be phosphorylated, and Ser 198 was reported to be important for NLRP3 priming²⁸. NLRP3 Thr 659 was not reported to be phosphorylated and, interestingly, the identified peptide appears to be conserved between humans and mice (Extended Data Fig. 6d). Reinforcing the potential conservation of the Pak–NLRP3 axis, CNF1-triggered caspase-1 activation was observed in primary human macrophages and was inhibited by treatment with NLRP3 inhibitor or Pak1 inhibitor (Extended Data Fig. 7a,b). In the inflammasome reconstitution system, we next expressed the activated Pak1^{T423E} and compared the effect of the expression of NLRP3 WT with the triple-mutant NLRP3^{S163A S198A T659A} or single mutants NLRP3^{S163A}, NLRP3^{S198A} and

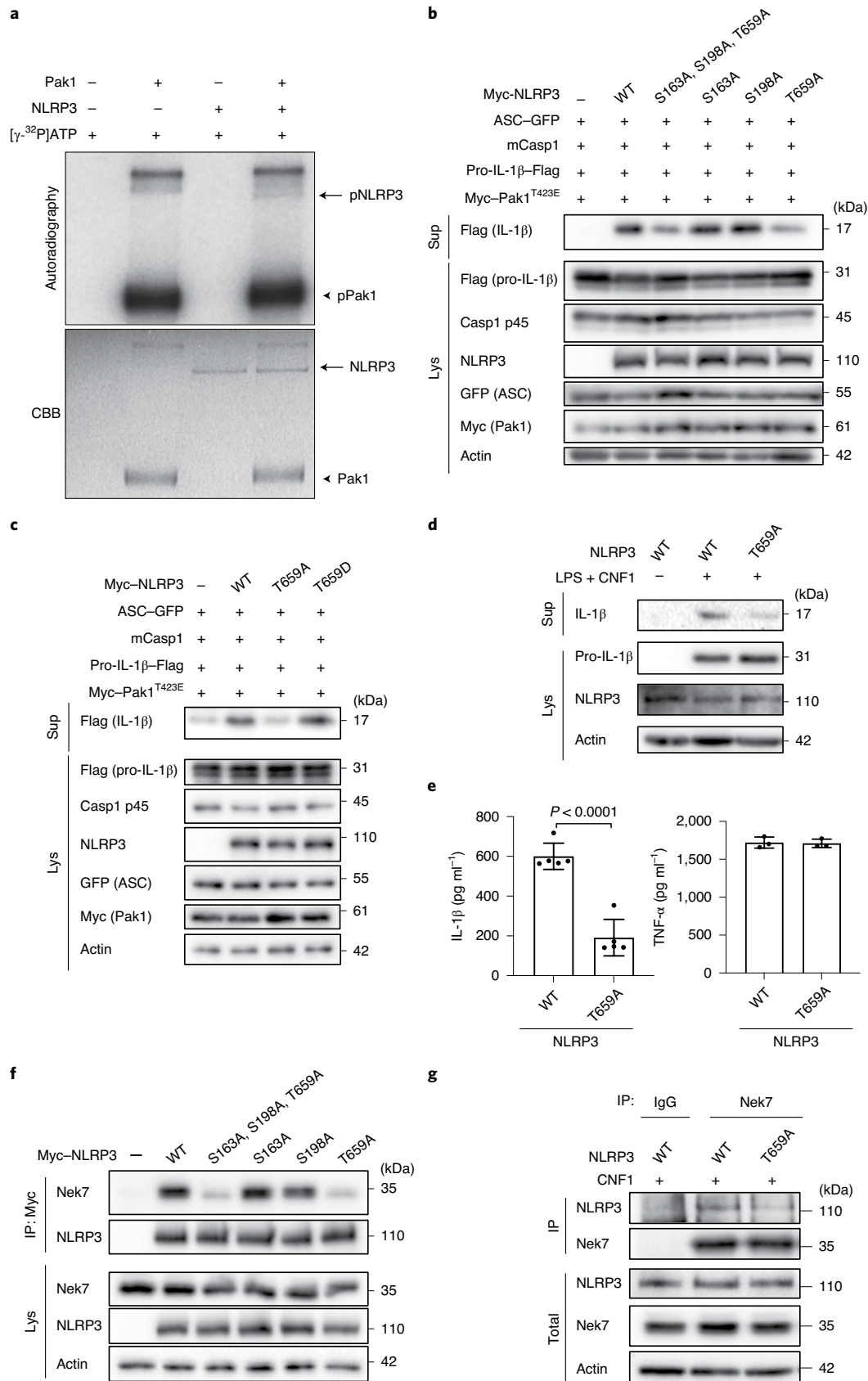
NLRP3^{T659A} in which the phosphorylated residues were replaced with alanine residues, which are not sensitive to phosphorylation. The results show that the triple-mutant NLRP3^{S163A S198A T659A} and the single mutant NLRP3^{T659A} is impaired in IL-1 β maturation triggered by the activated Pak1^{T423E}, indicating that the NLRP3 Thr 659 residue has an important role in Pak1-triggered NLRP3 inflammasome activation (Fig. 4b). Furthermore, we generated a T659D phosphomimetic NLRP3 mutant and observed that, compared with NLRP3^{T659A}, the NLRP3^{T659D} mutant had an increased ability to trigger pro-IL-1 β maturation (Fig. 4c). Importantly, similar results were obtained when the Rho-GTPase-activating virulence factor SopE was transfected to activate the pathway, highlighting the involvement of this NLRP3 post-translational regulation for the sensing of other virulence factors activating Rho GTPases (Extended Data Fig. 8a). We next stably reconstituted immortalized macrophages knocked-out for NLRP3 with plasmids encoding either NLRP3 or NLRP3^{T659A}. Confirming our results, we observed impaired CNF1-triggered IL-1 β maturation/secretion in macrophages expressing NLRP3^{T659A} compared with macrophages expressing WT NLRP3 (Fig. 4d,e). By contrast, TNF- α was similarly secreted by macrophages expressing either NLRP3 or NLRP3^{T659A} (Fig. 4e). After treatment with the DNT toxin, we also observed an impairment in CNF1-triggered IL-1 β maturation in macrophages expressing the NLRP3^{T659A} mutant compared with macrophages expressing WT NLRP3 (Extended Data Fig. 8b). Reinforcing the importance of this NLRP3 phosphorylation site in the inflammasome activation process, nigericin-triggered IL-1 β maturation and secretion were reduced in macrophages expressing the NLRP3^{T659A} compared with the macrophages expressing NLRP3, whereas TNF- α secretion was unaffected (Extended Data Fig. 9). Taken together, these results show that phosphorylation of NLRP3 at Thr 659 has a functional role, and that Pak1 is a regulator of the NLRP3 inflammasome. Structural analysis of the NLRP3–Nek7 interaction revealed a putative interaction domain at the level of the Thr 659 of NLRP3 (ref. ²⁹). Using co-immunoprecipitation experiments, we tested whether the NLRP3^{S163A S198A T659A} triple mutant or NLRP3^{S163A}, NLRP3^{S198A} and NLRP3^{T659A} single mutants affected the interaction with endogenous Nek7. The interaction between NLRP3 and Nek7 was impaired in the NLRP3^{S163A S198A T659A} triple mutant and in the NLRP3^{T659A} mutant, indicating that Thr 659 is a critical site for NLRP3–Nek7 interaction and suggesting that the phosphorylation of NLRP3 at Thr 659 is important for the NLRP3–Nek7 interaction (Fig. 4f). This observation was confirmed using anti-Nek7 immunoprecipitation in macrophages in which we found a decrease in NLRP3^{T659A} binding to Nek7 compared with WT NLRP3 (Fig. 4g).

Clearance of CNF1-expressing *E. coli* during bacteraemia requires the Pak–NLRP3 signalling axis. We next addressed the relevance of the CNF1-triggered Pak–NLRP3 signalling axis during infection. We observed an increase in caspase-1 maturation when macrophages were infected with CNF1-expressing *E. coli* compared

Fig. 4 | Pak1 phosphorylates NLRP3 to promote inflammasome activation. **a**, In vitro [γ -³²P]ATP kinase assay using human recombinant NLRP3 (arrows) and human recombinant Pak1 (arrowheads) analysed using autoradiography and Coomassie brilliant blue (CBB) staining. **b**, HEK293T cells were transfected with plasmids encoding components of the NLRP3 inflammasome (ASC–GFP, mouse caspase-1), pro-IL-1 β –Flag, Myc–Pak1^{T423E}, with Myc–NLRP3, Myc–NLRP3^{S163A}, Myc–NLRP3^{S198A}, Myc–NLRP3^{T659A} or Myc–NLRP3^{S163A S198A T659A}, and IL-1 β maturation was analysed using immunoblotting. **c**, HEK293T cells were transfected with plasmids encoding components of the NLRP3 inflammasome (ASC–GFP, mouse caspase-1) and Myc–Pak1^{T423E}, with Myc–NLRP3, Myc–NLRP3^{T659A} or Myc–NLRP3^{T659D}, and IL-1 β maturation was analysed using immunoblotting. **d,e**, NLRP3-knockout iBMDMs that were reconstituted with either NLRP3 or NLRP3^{T659A} were treated with vehicle or LPS (100 ng ml⁻¹) and CNF1 (500 ng ml⁻¹) for 8 h. **d**, Supernatants and cell lysates were analysed using immunoblotting. **e**, Supernatants were analysed using ELISA for IL-1 β ($n = 4$ biologically independent samples) and TNF- α ($n = 3$ biologically independent samples). Data are mean \pm s.e.m. Statistical analyses were performed using two-tailed unpaired Student's *t*-tests. **f**, HEK293T cells were transfected with plasmids encoding Myc–NLRP3, Myc–NLRP3^{S163A}, Myc–NLRP3^{S198A}, Myc–NLRP3^{T659A} or Myc–NLRP3^{S163A S198A T659A}. Cell lysates were processed for anti-Myc immunoprecipitation and endogenous Nek7 was revealed using anti-Nek7 antibodies. **g**, NLRP3-knockout iBMDMs that were reconstituted with either NLRP3 or NLRP3^{T659A} were treated with CNF1 (500 ng ml⁻¹) for 6 h. Cell lysates were analysed using immunoprecipitation with anti-Nek7 antibodies or isotopic IgG. Experiments were repeated at least three times, and representative data are shown.

with the isogenic *E. coli* CNF1-knockout strain, and treatment with NLRP3 or Pak1 inhibitors decreased the caspase-1 cleavage triggered by the *E. coli* expressing CNF1 (Fig. 5a). Furthermore, IL-1 β secretion triggered by the CNF1-expressing *E. coli* was reduced when

bacteria were added to NLRP3-knockout macrophages (Fig. 5b). Furthermore, the secretion of IL-1 β triggered by CNF1-expressing *E. coli* in macrophages complemented with the NLRP3^{T659A} mutant was decreased compared with control macrophages expressing



NLRP3 (Fig. 5c). TNF- α secretion measured during infection with CNF1-expressing *E. coli* was not affected in macrophages that were isolated from NLRP3-knockout mice or macrophages expressing the NLRP3^{T659A} mutant (Fig. 5b,c). We previously demonstrated that the CNF1 toxin expressed by *E. coli* triggered both an immune response in vivo and bacterial clearance during bacteraemia¹¹. To investigate the role of Pak1 during CNF1-expressing *E. coli* bacteraemia, we used the Pak1 inhibitor AZ13711265, which blocks CNF1-triggered IL-1 β maturation (Supplementary Fig. 3) and is associated with good in vivo pharmacokinetic properties²⁷. We monitored the bacterial burden during bacteraemia in control mice or mice injected with AZ13711265. Mice bacteraemia was measured for each mouse at 4 h, 24 h and 48 h after infection (Fig. 5d). The bacterial clearance of CNF1-expressing *E. coli* was observed; no bacteria were detectable at 48 h in all of the control animals (Fig. 5d). We measured a statistically significant higher bacterial load at 48 h and 77% of the animals were found to be positive for bacteraemia in the mice that were injected with the Pak1 inhibitor, indicating that in vivo the inhibition of Pak1 is sufficient to inhibit the CNF1-expressing *E. coli* clearance (Fig. 5d). We next used an NLRP3 inhibitor, MCC950, which has been shown to be efficient in vivo³⁰. We monitored bacteraemia in mice injected with MCC950 compared with the controls. The bacterial clearance of CNF1-expressing *E. coli* in mice injected with the NLRP3 inhibitor was significantly higher at 48 h, and 70% of the animals were found to be positive for bacteraemia (Fig. 5d). Consistent with our model, we observed no significant effect of both AZ13711265 and MCC950 towards the bacterial clearance when we infected mice with the isogenic *E. coli* CNF1-knockout strain (Extended Data Fig. 10a). To genetically prove this point, we infected WT mice, NLRP3-knockout mice or Pak1-knockout mice, and compared the CNF1-expressing *E. coli* burden. Consistent with the results obtained with the NLRP3 and Pak1 inhibitors, we did not detect any bacteria in the blood of infected WT mice at 48 h, whereas we measured a mean of 1.5×10^4 and 2.5×10^2 bacteria per mouse in the blood of NLRP3-knockout and Pak1-knockout mice, respectively (Fig. 5e,f). The smaller effect observed in Pak1-knockout mice compared with NLRP3-knockout mice could be explained by the redundancy observed between Pak1 and Pak2 at the cellular level. The difference in the clearance of CNF1-expressing *E. coli* measured at 48 h between WT and NLRP3-knockout mice was still observable at later time points and was not observed when mice were infected with the isogenic *E. coli* CNF1-knockout strain, indicating the specificity of the CNF1 response towards the NLRP3 pathway in vivo (Extended Data Fig. 10b,c). Furthermore, we measured a similar trend in the clearance of the CNF1-expressing *E. coli* strain in WT and GSDMD-knockout mice (Extended Data Fig. 10d). We next monitored the bacterial burden in mice that were infected with CNF1-expressing *E. coli* and treated with AZ13711265, MCC950 or both. We observed no differences in the bacterial clearance between the three groups (Fig. 5d). NLRP3-knockout mice that were injected with vehicle or with AZ13711265 demonstrated no differences in bacterial clearance, suggesting that Pak1 and NLRP3 act within the

same signalling pathway during bacteraemia (Fig. 5g). Together, these results unravel the critical role of Pak1 and NLRP3 in the clearance of CNF1-expressing bacteria and their importance in the innate immune response during bacteraemia.

Discussion

Our results shed light on a regulatory mechanism for NLRP3 after the activation of Rac2 by the bacterial toxin CNF1. The level of NLRP3 inflammasome activation is correlated with the strength of the interaction between activated Rac2 and Pak1-RBD, indicating that the innate immune system can adapt its response to the level of Rac2 activity. This seems to be an elegant strategy to deliver a commensurate response to the level of CNF1 toxin activity. Notably, the phosphorylated peptide containing Thr 659 of human NLRP3 isolated by mass spectrometry is highly conserved between species, and the Pak–NLRP3 axis is conserved in human macrophages and is involved in the nigericin-triggered NLRP3 inflammasome activation. Complementary studies will be necessary to determine the precise molecular mechanism in other species or in other contexts as well as to determine whether the phosphorylation of NLRP3 at Thr 659 is a consensus site used by other kinases. Nevertheless, our results show that phosphorylation of NLRP3 at Thr 659 is important for NLRP3 inflammasome activation and suggest that it is implicated in NLRP3-related inflammatory disorders or susceptibility to infection.

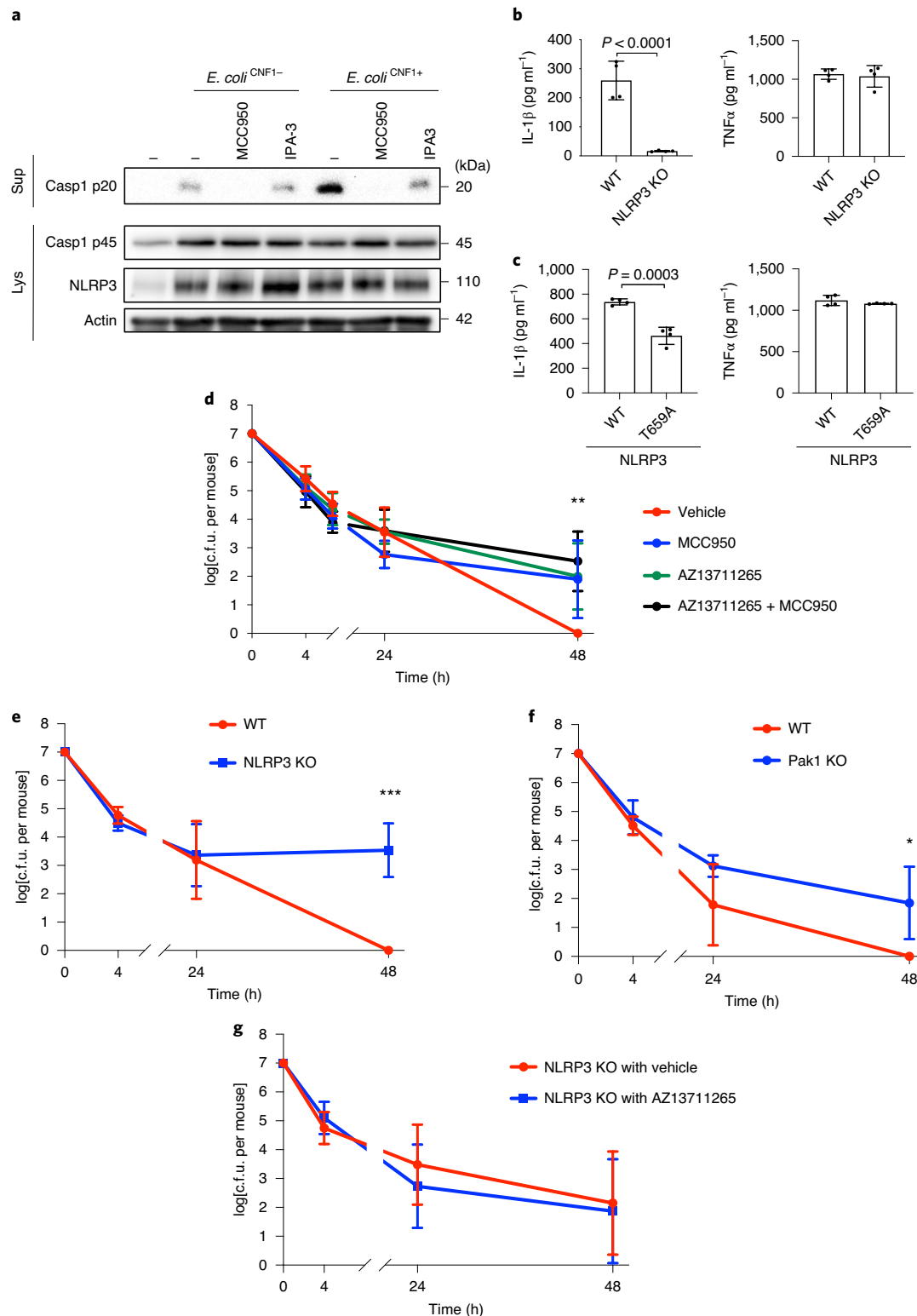
Our results suggest that there is redundancy between Pak1 and Pak2, as shown by a partial compensation by Pak2 in Pak1-knockout macrophages and mice. Further studies are required to clarify the importance of each of the group-1 Pak proteins in the activation of the NLRP3 inflammasome. Unfortunately, the Pak2-knockout mutations in mice are embryonically lethal (at embryonic day 8.0) and these studies would require the generation of conditional transgenic mice³¹.

We unravelled a CNF1-triggered secretion of IL-1 β that is not linked to an increase in cell death and is independent of GSDMD. Studies of NLRP3 inflammasome canonical triggers have demonstrated different IL-1 β secretion scenarios. In the conventional scenario, caspase-1 cleaves the inflammasome-related cytokines and GSDMD to generate active N-GSDMD^{32,33}. N-GSDMD relocates in the plasma membrane to form pores, enabling IL-1 β secretion^{32,33}. GSDMD pores are associated with pyroptosis in the case of classical inflammasome activation or are controlled during inflammasome hyperactivation, leading to secretion without pyroptosis^{34–36}. The CNF1-triggered IL-1 β secretion seems to fall into another category, independent of both GSDMD cleavage and cell death, that may share similarities with the unconventional IL-1 β secretion³⁷. This unconventional secretion relies on the affinity of IL-1 β to the plasma membrane ruffles that are characteristic of the CNF1-triggered Rac GTPase activation. The mechanism explaining how CNF1 triggered caspase-1 activation without GSDMD cleavage remains to be elucidated and may be unique to toxins activating Rho GTPases. One hypothesis is that the activation of Rac2, in parallel to the

Fig. 5 | Pak1 and NLRP3 control the burden of CNF1-expressing *E. coli* during bacteraemia. **a**, BMDMs isolated from C57BL/6 mice were pretreated for 45 min with 1 μ M MCC950 or 5 μ M IPA-3 and were infected or not (multiplicity of infection (m.o.i.) = 5) with either *E. coli*^{CNF1+} or isogenic CNF1-deleted mutant *E. coli*^{CNF1-}. Supernatants and cell lysates were analysed using immunoblotting. **b,c**, BMDMs isolated from C57BL/6 or C57BL/6 NLRP3-knockout mice (**b**) or iBMDMs expressing NLRP3 or NLRP3^{T659A} (**c**) were infected (m.o.i. = 5) with *E. coli*^{CNF1+}. The supernatants were analysed using ELISA. $n = 4$ biologically independent samples per group. Data are mean \pm s.e.m. Statistical analyses were performed using two-tailed unpaired Student's *t*-tests. **d–g**, Mice were intravenously infected with 10^7 colony-forming units (c.f.u.) of *E. coli*^{CNF1+}, before collecting peripheral blood at 4 h, 24 h and 48 h for the measurement of bacteraemia. **d**, C57BL/6J mice were injected intraperitoneally with vehicle, or with 50 mg kg⁻¹ MCC950 ($n = 10$ mice), 10 mg kg⁻¹ AZ13711265 ($n = 10$ mice) or both once a day ($n = 9$ mice). ** $P < 0.01$ (each individual inhibitor-treated group compared with the group injected with vehicle). **e**, WT ($n = 7$ mice) or NLRP3-knockout C57BL/6J mice ($n = 6$ mice) were analysed. *** $P < 0.001$. **f**, WT ($n = 4$ mice) or Pak1-knockout C57BL/6J mice were analysed ($n = 4$ mice). * $P < 0.05$. **g**, NLRP3-knockout C57BL/6J mice were injected intraperitoneally with 10 mg kg⁻¹ AZ13711265 ($n = 7$ mice) or vehicle ($n = 9$ mice) once each day. Experiments were repeated at least two times, and representative data are shown. Data are the geometric mean \pm 95% confidence interval. Statistical analyses were performed using two-tailed nonparametric Mann-Whitney *U*-tests. * $P < 0.05$, ** $P < 0.01$, *** $P < 0.001$.

Pak1–NLRP3 pathway activation, inhibits the cleavage of GSDMD. Similar to *Toxoplasma gondii*, the NF- κ B activation triggered by Rac2 might be another mechanism explaining the IL-1 β secretion independent of cell death and GSDMD³⁸. Rac2 signalling may also regulate a potassium channel explaining the inhibition by KCl of the CNF1-triggered IL-1 β secretion. Favouring this hypothesis, Rac GTPases have been found to modulate Kir2.1, a Kir-family potassium channel³⁹.

Our study shows that NLRP3 is a major sensor of toxins that activate Rho GTPases, whereas previous research has shown the sensing of Rho-GTPase-inactivating toxins by Pyrin¹². These studies highlight that the mammalian innate immune system has evolved strategies that share similarities with the effector-triggered immunity to detect abnormal activation of Rho GTPases^{3,40,41}. Interestingly, both inactivation of RhoA and activation of Rac2 by bacterial toxins are monitored by Pyrin and NLRP3, respectively. More precisely,



here we show that Rac GTPases that activate bacterial factors are sensed by NLRP3 independently of the type of modification made. Similarly, bacterial factors that inactivate RhoA activate Pyrin independently of the type of modifications^{12,42,43}. These results suggest that the host guarding of Rho GTPase signalling integrity relies on two sensors that monitor the abnormal Rho GTPase cycling rather than toxin-triggered post-translational modifications of host proteins or virulence factor enzymatic activities. Interestingly, both Pyrin and NLRP3 require regulation by the serine–threonine kinases PKN1/2 and Pak1/2, respectively. The fact that two different inflammasomes have been evolutionarily selected to detect bacterial toxins that modify Rho GTPases highlights the importance of Rho GTPases in innate immunity.

Further studies are necessary to determine the *in vivo* conservation of the Pak–NLRP3 axis and whether the sensing of other Rho–GTPase-activating virulence factors by the NLRP3 inflammasome impacts the bacterial burden during infection. Similarly, we expect that further studies will determine the importance of other inflammasomes in detecting bacterial virulence factors that are endowed with enzymatic activities.

Our results reveal the importance of Pak1 and NLRP3 in controlling the bacterial burden during bacteraemia in mice. Even though further studies will be required to determine the role of the Pak–NLRP3 signalling axis in patients with bacteraemia, our results showing an increase in bacterial burden in MCC950-treated mice suggest that caution will be necessary for the use of NLRP3 inhibitors in the clinical setting. This is consistent with clinical data showing that there is an increased risk of infections associated with IL-1 signalling inhibition^{44,45}. One option would be to consider combining inflammasome inhibitors with antibiotherapies or with an enhanced surveillance for a potential for bacteraemia risk.

Methods

Ethics statement. This study was carried out in strict accordance with the guidelines of the Council of the European Union (Directive 86/609/EEC) regarding the protection of animals used for experimental and other scientific purposes. The protocol was approved by the Institutional Animal Care and Use Committee on the Ethics of Animal Experiments of Nice, France (APAFIS#18322-20181218099427035 v2 and APAFIS#24906-2020031614223228 v2).

Bacterial strains and toxins. The *E. coli* UTI89 clinical isolate was originally obtained from a patient with cystitis⁴⁶ and the isogenic UTI89 CNF1⁺ (*E. coli*^{CNF1+}) or UTI89 CNF1⁻ (*E. coli*^{CNF1-}) streptomycin-resistant strain generation and culture conditions were previously described⁴¹. For the infections, a 1/100 dilution of an overnight culture was inoculated and grown up to an optical density at 600 nm of 1.2 using a Luria–Bertani (LB) medium supplemented with streptomycin (200 µg ml⁻¹). Bacteria were collected by centrifugation and washed twice in PBS before dilution in PBS to obtain the desired bacterial concentrations for the mouse infection experiments. Recombinant WT CNF1 and its catalytically inactive form (CNF1^{C866S}) were produced and purified as previously reported^{47,48}. The recombinant DNT toxin was purified from pQEDNTwt using the same protocol⁴⁹. The recombinant proteins were passed through a polymyxin B column (Affinity Detoxi-Gel, Pierce). The removal of endotoxin was verified using a colorimetric limulus amoebocyte lysate (LAL) assay (LAL QCL-1000, Cambrex). Each stock of the CNF1 preparation (2 mg ml⁻¹) was shown to contain less than 0.5 endotoxin units per ml. Plasmid expressing the virulence factor pCMV-SopE-HA was previously reported²² and SopE expression was stabilized by adding MG132 (10 µM) to the cells to block its proteasomal degradation as previously described⁵⁰. Plasmids expressing the PRK5-Myc-DNT were obtained by PCR amplification of pQEDNTwt, and pCMV-HA-YopE was obtained by PCR amplification and subcloning from pACY184-YopE-GSK (gift from I. Brodsky). All of the plasmids were verified by sequencing (Eurofins).

Cell culture, transfection and inhibitors. HEK293T cells were obtained from ATCC (CRL-3216) and maintained according to the ATCC instructions. BMDMs were extracted from the femurs of BALB/c, C57BL/6J, C57BL/6J knockout or C57BL/6J knockout mice (aged 6–10 weeks) as indicated in the legends and were cultured in RPMI GlutaMax medium (Life Technologies) supplemented with 100 ng ml⁻¹ M-CSF (premium grade, Miltenyi Biotec), 10% heat-inactivated FBS (Biowest) and 50 µg ml⁻¹ gentamycin (Life Technologies) at 37 °C in an atmosphere containing 5% CO₂. The cells were seeded at a concentration of 10⁶ cells per well in a six-well plate. After 6 d of differentiation, BMDMs were used for

experiments. HEK293T cells were transfected with plasmids using Lipofectamine 2000 (Life Technologies) according to the manufacturer's instructions. siRNAs were transfected in BMDMs for 72 h using Lipofectamine RNAiMAX Reagent (Thermo Fisher Scientific) according to the manufacturer's instructions. Cells were transfected as indicated in the figure legends with siRNAs (Dharmacon) targeting *Nlrp3* (L-053455-00), *Rac1* (L-041170-00), *Rac2* (L-041171-01), *Nek7* (J-063266-09), *Pak1* (L-048101-00), *Pak2* (L-040615-00) or non-targeting control siRNA (D-001810-10). For the siRNA screen, the BMDMs were transfected with siRNA (Dharmacon) targeting *Nod1* (L-055182-00), *Nod2* (L-052735-00), *Nlr3* (L-052823-01), *Nlr4* (L-055000-00), *Nlr5* (L-067620-01), *Nlr1* (L-057712-01), *Ciita* (L-043166-02), *Naip1* (L-047682-00), *Naip2* (L-044151-01), *Naip5* (L-044142-01), *Naip6* (L-044145-01), *Naip7* (L-065757-00), *Nlrp1a* (L-066229-00), *Nlrp1b* (L-161107-01), *Nlrp2* (L-053528-01), *Nlrp3* (L-053455-01), *Nlrp4a* (L-052395-01), *Nlrp4b* (L-058181-01), *Nlrp4c* (L-049416-01), *Nlrp4d* (L-067051-01), *Nlrp4e* (L-068064-01), *Nlrp4f* (L-052668-01), *Nlrp4g* (L-066364-01), *Nlrp5* (L-045315-01), *Nlrp6* (L-066157-01), *Nlrp9a* (L-058269-01), *Nlrp9b* (L-066417-01), *Nlrp9c* (L-057344-01), *Nlrp10* (L-056559-01), *Nlrp12* (L-060234-01), *Nlrp14* (L-066093-01), *Pycard* (L-051439-01), *Mefv* (L-048693-01) and *Aim2* (L-044968-01). BMDMs were pretreated with the following inhibitors for 45 min: 1 µM CP-456773 or MCC950 (Sigma-Aldrich), 5 µM IPA-3 (Tocris), 1 µM FRAX597 (Tocris) or the indicated concentration of AZ13711265 (AGV Discovery) in 2% FBS containing RPMI followed by the addition of CNF1 500 ng ml⁻¹ and/or ultrapure LPS 100 ng ml⁻¹ (Invivogen) as indicated in the figure legends. Cells treated with nigericin 5 µM (Invivogen) or ATP 5 mM (Invivogen) for 30 min were used as positive control for NLRP3 inflammasome activation. For K⁺-efflux-preventing experiments, BMDMs were treated with 10 mM, 20 mM or 40 mM KCl. Primary macrophages were infected with *E. coli*^{CNF1+} or the isogenic *E. coli*^{CNF1-} (m.o.i. = 5) for 16 h. Immortalized NLRP3-knockout BMDMs were stably complemented with pINDUCER2.1 plasmids encoding human NLRP3 WT or NLRP3^{T659A} under a doxycycline-inducible promoter as previously described⁵¹. NLRP3 expression was induced by adding 2 µg ml⁻¹ doxycycline for 16 h (Takara Bio). All of the cell lines were authenticated using PCR assays with species-specific primers. Mycoplasma testing was negative.

Mouse model of infection. Female C57BL/6J mice (aged 7 weeks; Charles River Laboratory) were injected intraperitoneally with MCC950 (Sigma-Aldrich) at 50 mg kg⁻¹ every 24 h or AZ13711265 (AGV Discovery) at 10 mg kg⁻¹ every 24 h or both. NLRP3-knockout mice were provided by V. Petrilli and were described previously⁵². The Pak1-knockout, GSDMD-knockout and ASC–citricine-knockin mice used in this study were reported previously^{17,32,53}. Female NLRP3-knockout or Pak1-knockout and female congenic WT C57BL/6J littermate mice were injected intravenously with 10⁷ colony-forming units of *E. coli* and the determination of bacteraemia was monitored as previously described⁴¹. Mice were housed with their littermates and kept under a regular 12 h–12 h light–dark cycle at room temperature (20–25 °C) and a relative humidity of 50–70%. Food and water were available *ad libitum*. Experiments were performed under pathogen-free conditions with randomly chosen animals (same sex, matched by age and body weight). Investigators were blinded for *in vivo* experiments. Sample size was determined on the basis of our previous research⁴¹ and using G*Power software.

Reconstituted NLRP3 inflammasome in HEK293T cells. HEK293T cells were transfected with plasmids encoding the NLRP3 inflammasome components as previously described^{11,28}. HEK293T cells were transfected with plasmids encoding Myc–NLRP3 or NLRP3 mutants, ASC–GFP, mpro-caspase1 and pro-IL-1β–Flag. Where indicated in the legend, cells were cotransfected with HA–Rac2, the constitutively active mutant of Rac2 mimicking CNF1-induced deamidation Rac2^{Q61E}, Rac2^{Q61L}, Rac2^{G12V} or Rac2^{T17N}, a dominant negative mutant of Rac2 for 16 h. The monitoring of caspase-1 or IL-1β cleavage was performed using supernatant immunoblotting.

Immunoprecipitation. HEK293T cells were transfected with plasmids encoding Myc–NLRP3, Myc–NLRP3^{S163A/S198A/T659A}, Myc–NLRP3^{S163A} and Myc–NLRP3^{T659A}, GFP–NLRP3, Myc–Pak1^{T423E} and HA–Rac2^{Q61E}, or NLRP3 expression was induced by adding 2 µg ml⁻¹ doxycycline for 16 h to iBMDMs stably expressing NLRP3 or NLRP3^{T659A}. Cells were lysed and processed for immunoprecipitation using 2 µg of anti-Myc or 3 µg of anti-Nek7 antibodies according to previously described conditions⁵⁴. The expression of NLRP3 and endogenous levels of Nek7 were monitored in the cell lysate as well as in the immunoprecipitated fraction.

LDH release. The supernatant of stimulated macrophages was collected and centrifuged at 300g for 5 min to remove cellular debris. LDH measurement was performed using the LDH Cytotoxicity Assay Kit (Thermo Fisher Scientific) according to the manufacturer's instructions, in samples diluted 1:5 in PBS. Data were plotted as the percentage of LDH release considering a Triton X-100 treated well as 100%.

Cell permeabilization kinetics. BMDMs were plated and stimulated in a 96-well plate in medium containing propidium iodide (0.1 µg ml⁻¹) and data were acquired with a ×10 objective using the InCyte Zoom system v.6.2.9200.0

(Essen BioScience) under a CO₂- and temperature-controlled environment. Each condition was run in quadruplicate. The number of fluorescent objects was counted using Incucyte Zoom (Essen BioScience).

In vitro kinase assay. Recombinant purified Pak1 (500 ng) was incubated with 1 µg of recombinant human NLRP3 protein (Abcam, ab165022), and with 50 µM ATP and 4 µCi of [³²P]ATP in kinase buffer (50 mM HEPES pH 7.3, 50 mM NaCl, 0.05% Triton X-100, 10 mM β-glycerophosphate, 5 mM NaF, 10 mM MgCl₂ and 0.2 mM MnCl₂) at 30°C for 30 min in a final volume of 39 µl. The reaction was stopped by adding 15 µl of LDS (Thermo Fisher Scientific) and 6 µl of dithiothreitol 500 mM. Samples were analysed by electrophoresis using Bolt 4–12% Bis-Tris Plus gels (Thermo Fisher Scientific) followed by Coomassie blue staining and autoradiography.

Immunofluorescence staining, antibodies and ELISA assays. Caspase-1 activation was detected using the fluorescent probe FAM-FLICA (ImmunoChemistry Technologies) after 6 h of treatment, according to the manufacturer's instructions. After labelling, cells were fixed in 4% paraformaldehyde for 15 min, PFA was neutralized with 50 mM NH₄Cl for 15 min, cells were permeabilized with 0.5% Triton X-100 for 5 min and blocked with 2% TBS-BSA. Cells were incubated with mouse anti-NLRP3 (clone Cryo-2, Adipogen) and/or rabbit anti-ASC (AG-25B-0006, Adipogen) or rabbit anti-phosphorylated-Pak (ab40795, Abcam) antibodies for 1 h followed by incubation with the secondary antibodies TexasRed anti-mouse IgG (TI-2000, Vector Laboratories) or Cy5 anti-mouse IgG (715-175-151, Jackson ImmunoResearch) and/or TexasRed anti-rabbit IgG (711-075-152, Jackson ImmunoResearch) and/or phalloidin Alexa Fluor 647 (ab176759, Abcam) and Hoechst 33342 (H1399, Thermo Fisher Scientific) for 30 min. Cells were imaged using a Nikon A1R confocal microscope. The following antibodies were used in this study: rabbit anti-IL-1β (GTX74034, Genetex), mouse anti-caspase-1 (clone Casper-1, Adipogen), mouse anti-Rac (clone 102/Rac1, BD Biosciences), goat anti-Rac2 (ab2244, Abcam), mouse anti-NLRP3 (clone Cryo-2, Adipogen), rabbit anti-Nek7 (ab133514, Abcam), rabbit anti-Pak1 (2602, CST), rabbit anti-Pak2 (2608, CST), rabbit monoclonal anti-GSDMD (ab209845), mouse anti-β-actin (AC-74, Sigma-Aldrich), mouse anti-Myc (9E10, Roche), mouse anti-HA (16B12, Covance), mouse anti-Flag (clone M2, Sigma-Aldrich), mouse anti-GFP (clone 7.1, 13.1, Roche). Cytokine secretion was determined by ELISA using the mouse Quantikine ELISA kits for mouse IL-6, IL-18, TNF-α and IL-1β (R&D Systems) according to the manufacturer's instructions.

Flow cytometry analysis. BMDMs isolated from C57BL/6J mice constitutively expressing ASC–citrine fusion protein (R26-CAG-ASC–citrine) were treated with LPS (100 ng ml⁻¹) for 16 h before 6 h of treatment with vehicle or CNF1 (500 ng ml⁻¹) or 30 min with nigericin (5 µM). Cells were collected and analysed by flow cytometry using a BD FACSCanto II cytometer (BD Biosciences). Cytometry data were analysed using FlowJo v.10.6.2. Doublets were excluded using a side scatter (SSC)-A (area) and SSC-H (height) plot; cells with a high expression of ASC–citrine were gated and then analysed for ASC–citrine signal area (ASC–citrine-A) and ASC–citrine signal height (ASC–citrine-H). Cells with ASC specks were defined with a higher ASC-H:ASC-A ratio.

Statistical analyses. Statistical analyses were performed using GraphPad Prism v.8.2.1. Comparisons of the bacterial load of mice were performed using nonparametric Mann–Whitney *U*-tests. Statistical analyses of FAM-FLICA⁺ cells, cytokine secretion and LDH release were performed using unpaired two-tailed Student's *t*-tests.

Reporting Summary. Further information on research design is available in the Nature Research Reporting Summary linked to this article.

Data availability

All data supporting the findings of this study are available within the Article and its Supplementary Information or from the corresponding author on reasonable request. Source data are provided with this paper.

Received: 21 August 2019; Accepted: 13 November 2020;

Published online: 11 January 2021

References

- Martin, G. S., Mannino, D. M., Eaton, S. & Moss, M. The epidemiology of sepsis in the United States from 1979 through 2000. *N. Engl. J. Med.* **348**, 1546–1554 (2003).
- Vance, R. E., Isberg, R. R. & Portnoy, D. A. Patterns of pathogenesis: discrimination of pathogenic and nonpathogenic microbes by the innate immune system. *Cell Host Microbe* **6**, 10–21 (2009).
- Stuart, L. M., Paquette, N. & Boyer, L. Effector-triggered versus pattern-triggered immunity: how animals sense pathogens. *Nat. Rev. Immunol.* **13**, 199–206 (2013).
- Flatau, G. et al. Toxin-induced activation of the G protein p21 Rho by deamidation of glutamine. *Nature* **387**, 729–733 (1997).
- Schmidt, G. et al. Gln63 of Rho is deamidated by *Escherichia coli* cytotoxic necrotizing factor-1. *Nature* **387**, 725–729 (1997).
- Aktories, K. & Barbieri, J. Bacterial cytotoxins: targeting eukaryotic switches. *Nat. Rev. Microbiol.* **3**, 397–410 (2005).
- Galán, J. E. Common themes in the design and function of bacterial effectors. *Cell Host Microbe* **5**, 571–579 (2009).
- Bruno, V. M. et al. *Salmonella* Typhimurium type III secretion effectors stimulate innate immune responses in cultured epithelial cells. *PLoS Pathog.* **5**, e1000538 (2009).
- Munro, P. et al. Activation and proteasomal degradation of Rho GTPases by cytotoxic necrotizing factor-1 elicit a controlled inflammatory response. *J. Biol. Chem.* **279**, 35849–35857 (2004).
- Boquet, P. & Lemichez, E. Bacterial virulence factors targeting Rho GTPases: parasitism or symbiosis? *Trends Cell Biol.* **13**, 238–246 (2003).
- Diabate, M. et al. *Escherichia coli* α-hemolysin counteracts the anti-virulence innate immune response triggered by the Rho GTPase activating toxin CNF1 during bacteremia. *PLoS Pathog.* **11**, e1004732 (2015).
- Xu, H. et al. Innate immune sensing of bacterial modifications of Rho GTPases by the pyrin inflammasome. *Nature* **513**, 237–241 (2014).
- Gros Lambert, M. & Py, B. F. Spotlight on the NLRP3 inflammasome pathway. *J. Inflamm. Res.* **11**, 359–374 (2018).
- Yang, Y., Wang, H., Kouadir, M., Song, H. & Shi, F. Recent advances in the mechanisms of NLRP3 inflammasome activation and its inhibitors. *Cell Death Dis.* **10**, 128 (2019).
- Gao, W., Yang, J., Liu, W., Wang, Y. & Shao, F. Site-specific phosphorylation and microtubule dynamics control pyrin inflammasome activation. *Proc. Natl Acad. Sci. USA* **113**, E4857–E4866 (2016).
- Park, Y. H., Wood, G., Kastner, D. L. & Chae, J. J. Pyrin inflammasome activation and RhoA signaling in the autoinflammatory diseases FMF and HIDS. *Nat. Immunol.* **17**, 914–921 (2016).
- Tzeng, T. C. et al. A fluorescent reporter mouse for inflammasome assembly demonstrates an important role for cell-bound and free ASC specks during in vivo infection. *Cell Rep.* **16**, 571–582 (2016).
- Sester, D. P. et al. Assessment of inflammasome formation by flow cytometry. *Curr. Protoc. Immunol.* **114**, 14.40.1–14.40.29 (2016).
- Lamkanfi, M. & Dixit, V. M. In retrospect: the inflammasome turns 15. *Nature* **548**, 534–535 (2017).
- He, Y., Hara, H. & Núñez, G. Mechanism and regulation of NLRP3 inflammasome activation. *Trends Biochem. Sci.* **41**, 1012–1021 (2016).
- Shi, H., Murray, A. & Beutler, B. Reconstruction of the mouse inflammasome system in HEK293T cells. *Bio. Protoc.* **6**, e1986 (2016).
- Keestra, A. M. et al. Manipulation of small Rho GTPases is a pathogen-induced process detected by NOD1. *Nature* **496**, 233–237 (2013).
- Doye, A. et al. CNF1 exploits the ubiquitin-proteasome machinery to restrict Rho GTPase activation for bacterial host cell invasion. *Cell* **111**, 553–564 (2002).
- Boyer, L. et al. Pathogen-derived effectors trigger protective immunity via activation of the Rac2 enzyme and the IMD or Rip kinase signaling pathway. *Immunity* **35**, 536–549 (2011).
- Manser, E., Leung, T., Salihuddin, H., Zhao, Z. S. & Lim, L. A brain serine/threonine protein kinase activated by Cdc42 and Rac1. *Nature* **367**, 40–46 (1994).
- Wells, C. M. & Jones, G. E. The emerging importance of group II PAKs. *Biochem. J.* **425**, 465–473 (2010).
- Semenova, G. & Chernoff, J. Targeting PAK1. *Biochem. Soc. Trans.* **45**, 79–88 (2017).
- Song, N. et al. NLRP3 phosphorylation is an essential priming event for inflammasome activation. *Mol. Cell* **68**, 185–197 (2017).
- Sharif, H. et al. Structural mechanism for NEK7-licensed activation of NLRP3 inflammasome. *Nature* **570**, 338–343 (2019).
- Coll, R. C. et al. A small-molecule inhibitor of the NLRP3 inflammasome for the treatment of inflammatory diseases. *Nat. Med.* **21**, 248–255 (2015).
- Kelly, M. L. & Chernoff, J. Mouse models of PAK function. *Cell Logist.* **2**, 84–88 (2012).
- Shi, J. et al. Cleavage of GSDMD by inflammatory caspases determines pyroptotic cell death. *Nature* **526**, 660–665 (2015).
- He, W. T. et al. Gasdermin D is an executor of pyroptosis and required for interleukin-1β secretion. *Cell Res.* **25**, 1285–1298 (2015).
- Broz, P., Pelegrín, P. & Shao, F. The gasdermins, a protein family executing cell death and inflammation. *Nat. Rev. Immunol.* **20**, 143–157 (2020).
- Rühl, S. et al. ESCRT-dependent membrane repair negatively regulates pyroptosis downstream of GSDMD activation. *Science* **362**, 956–960 (2018).
- Evavold, C. L. et al. The pore-forming protein gasdermin D regulates interleukin-1 secretion from living macrophages. *Immunity* **48**, 35–44 (2018).
- Monteleone, M. et al. Interleukin-1β maturation triggers its relocation to the plasma membrane for gasdermin-D-dependent and -independent secretion. *Cell Rep.* **24**, 1425–1433 (2018).

38. Pandori, W. J. et al. *Toxoplasma gondii* activates a Syk-CARD9-NF- κ B signaling axis and gasdermin D-independent release of IL-1 β during infection of primary human monocytes. *PLoS Pathog.* **15**, e1007923 (2019).
39. Muessel, M. J., Harry, G. J., Armstrong, D. L. & Storey, N. M. SDF-1 α and LPA modulate microglia potassium channels through rho GTPases to regulate cell morphology. *Glia* **61**, 1620–1628 (2013).
40. Jones, J. D. & Dangl, J. L. The plant immune system. *Nature* **444**, 323–329 (2006).
41. Lopes Fischer, N., Naseer, N., Shin, S. & Brodsky, I. E. Effector-triggered immunity and pathogen sensing in metazoans. *Nat. Microbiol.* **5**, 14–26 (2020).
42. Aubert, D. F. et al. A *Burkholderia* type VI effector deamidates Rho GTPases to activate the pyrin inflammasome and trigger inflammation. *Cell Host Microbe* **19**, 664–674 (2016).
43. Medici, N. P., Rashid, M. & Bliska, J. B. Characterization of pyrin dephosphorylation and inflammasome activation in macrophages as triggered by the yersinia effectors YopE and YopT. *Infect. Immun.* **87**, e00822-18 (2019).
44. Cabral, V. P., Andrade, C. A., Passos, S. R., Martins, M. F. & Hökerberg, Y. H. Severe infection in patients with rheumatoid arthritis taking anakinra, rituximab, or abatacept: a systematic review of observational studies. *Rev. Bras. Reumatol. Engl. Ed.* **56**, 543–550 (2016).
45. Ridker, P. M. et al. Antiinflammatory therapy with canakinumab for atherosclerotic disease. *N. Engl. J. Med.* **377**, 1119–1131 (2017).
46. Mulvey, M. A., Schilling, J. D. & Hultgren, S. J. Establishment of a persistent *Escherichia coli* reservoir during the acute phase of a bladder infection. *Infect. Immun.* **69**, 4572–4579 (2001).
47. Buetow, L., Flatau, G., Chiu, K., Boquet, P. & Ghosh, P. Structure of the Rho-activating domain of *Escherichia coli* cytotoxic necrotizing factor 1. *Nat. Struct. Biol.* **8**, 584–588 (2001).
48. Doye, A., Boyer, L., Mettouchi, A. & Lemichez, E. Ubiquitin-mediated proteasomal degradation of Rho proteins by the CNF1 toxin. *Methods Enzymol.* **406**, 447–456 (2006).
49. Matsuzawa, T., Kashimoto, T., Katahira, J. & Horiguchi, Y. Identification of a receptor-binding domain of *Bordetella* dermonecrotic toxin. *Infect. Immun.* **70**, 3427–3432 (2002).
50. Kubori, T. & Galán, J. E. Temporal regulation of salmonella virulence effector function by proteasome-dependent protein degradation. *Cell* **115**, 333–342 (2003).
51. Lagrange, B. et al. Human caspase-4 detects tetra-acylated LPS and cytosolic *Francisella* and functions differently from murine caspase-11. *Nat. Commun.* **9**, 242 (2018).
52. Martinon, F., Pétrilli, V., Mayor, A., Tardivel, A. & Tschopp, J. Gout-associated uric acid crystals activate the NALP3 inflammasome. *Nature* **440**, 237–241 (2006).
53. McDaniel, A. S. et al. *Pak1* regulates multiple c-Kit mediated Ras-MAPK gain-in-function phenotypes in *Nf1*^{+/-} mast cells. *Blood* **112**, 4646–4654 (2008).
54. Stutz, A. et al. NLRP3 inflammasome assembly is regulated by phosphorylation of the pyrin domain. *J. Exp. Med.* **214**, 1725–1736 (2017).

Acknowledgements

We thank P. Auberger, A. Baumler, I. Brodsky, J. Chernoff, D. Golenbock, T. Henry, M. Keestra-Gounder, E. Lemichez, E. Manser, E. Meunier, V. Petrilli, D. Pisani, J.-E. Ricci, G. Robert, P.-M. Roger, L. Stuart, P. Vandenabeele, S. Ivanov and L. Yvan-Charvet for sharing materials or discussions; A.-S. Dufour, E. Garcia, M. Irdelle and J. Murdaca for technical assistance; members of the Innate Sensors Community (InnaSCO) for sharing tools; A. Cuttriss and staff at the Office of International Scientific Visibility of Université Côte d'Azur for professional language editing; staff at the Etablissement Français du Sang of Marseille for providing human blood from human healthy donors; and staff at the C3M facilities (animal, genomic, cytometry and imaging) and the Harvard Taplin mass spectrometry core. The mouse strain used for this research project, B6.129S2-Pak1tm1Cher/Mmnc (RRID, MMRRRC_031838-UNC) was obtained from the Mutant Mouse Resource and Research Center (MMRRC) at University of North Carolina at Chapel Hill, an NIH-funded strain repository, and was donated to the MMRRRC by J. Chernoff, Fox Chase Cancer Center. This work was supported by grants from the ANR (ANR-17-CE15-0001), Investments for the Future programs LABEX SIGNALIFE ANR-11-LABX-0028-01, IDEX UCA^{EDU} ANR-15-IDEX-01, ARC (RAC15014AAA), Université Côte d'Azur, Infectiopole sud and REDPIT. B.F.P. is supported by ERC (ERC-2013-CoG_616986). A.M. is supported by a fellowship from FRM; C.T. by a fellowship from Ville de Nice; and O.D. by a fellowship from INSERM and Université Côte d'Azur.

Author contributions

O.D. and A.D. designed, performed and analysed most of the experiments with input from C.T., C.L., A.J., A.G., A.M., P.C., A.R. and S.M.; J.C. and R.R. provided advice on the mice infection model. E.V., R.R.G., D.C., B.F.P., A.R., P.H.V.S. and M.L. provided tools and advice on NLRP3 inflammasome regulation. P.M. generated NLRP3 mutants and, with G.M. and O.D., performed and analysed most of the in vivo experiments. O.V. performed virulence factor and toxin subcloning, protein purifications, the in vitro kinase assay and analysed the mass spectrometry results. L.B. conceived the project, designed experiments and wrote the manuscript.

Competing interests

The authors declare no competing interests.

Additional information

Extended data is available for this paper at <https://doi.org/10.1038/s41564-020-00832-5>.

Supplementary information is available for this paper at <https://doi.org/10.1038/s41564-020-00832-5>.

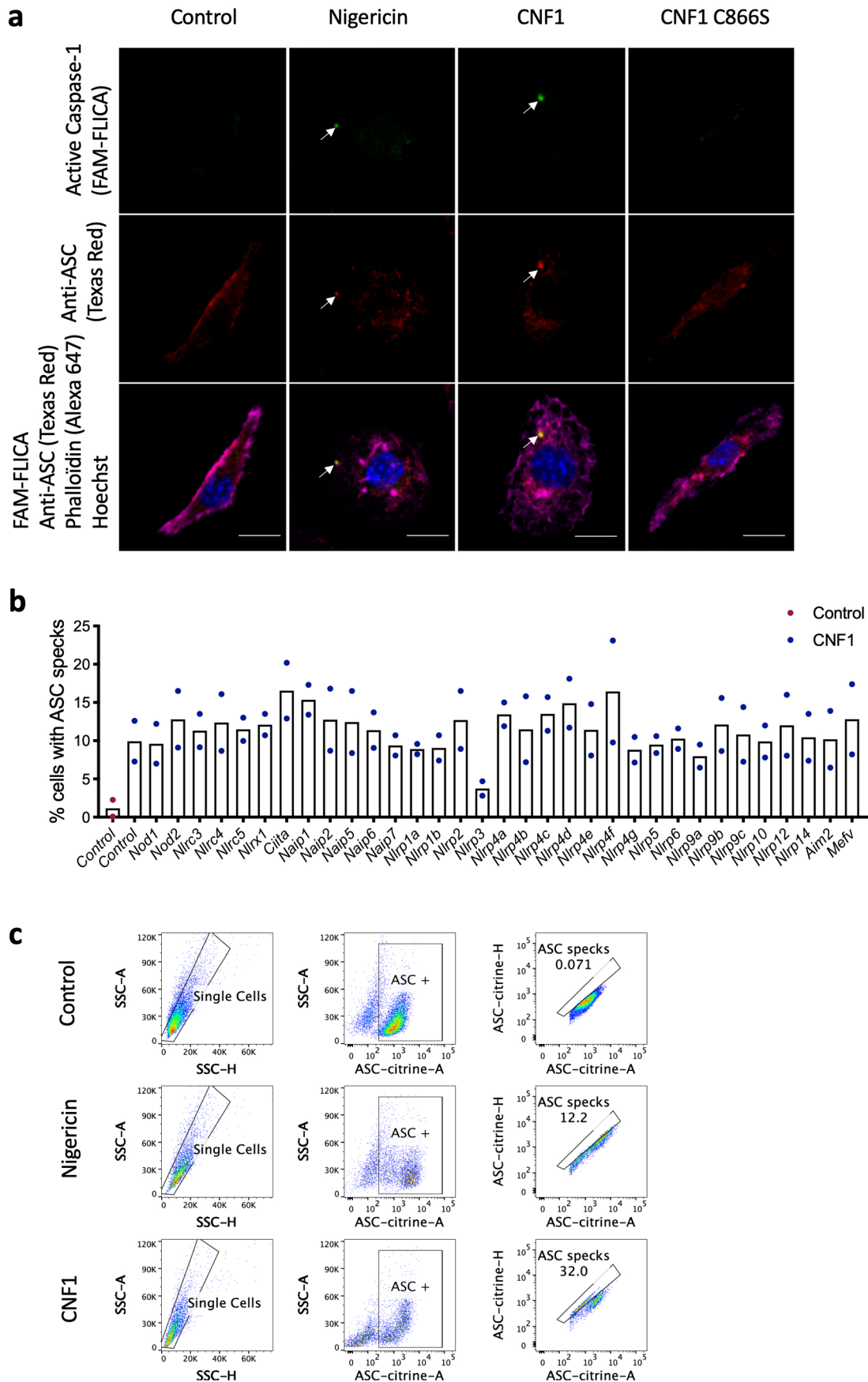
Correspondence and requests for materials should be addressed to L.B.

Peer review information *Nature Microbiology* thanks Igor Brodsky, Gad Frankel and the other, anonymous, reviewer(s) for their contribution to the peer review of this work.

Reprints and permissions information is available at www.nature.com/reprints.

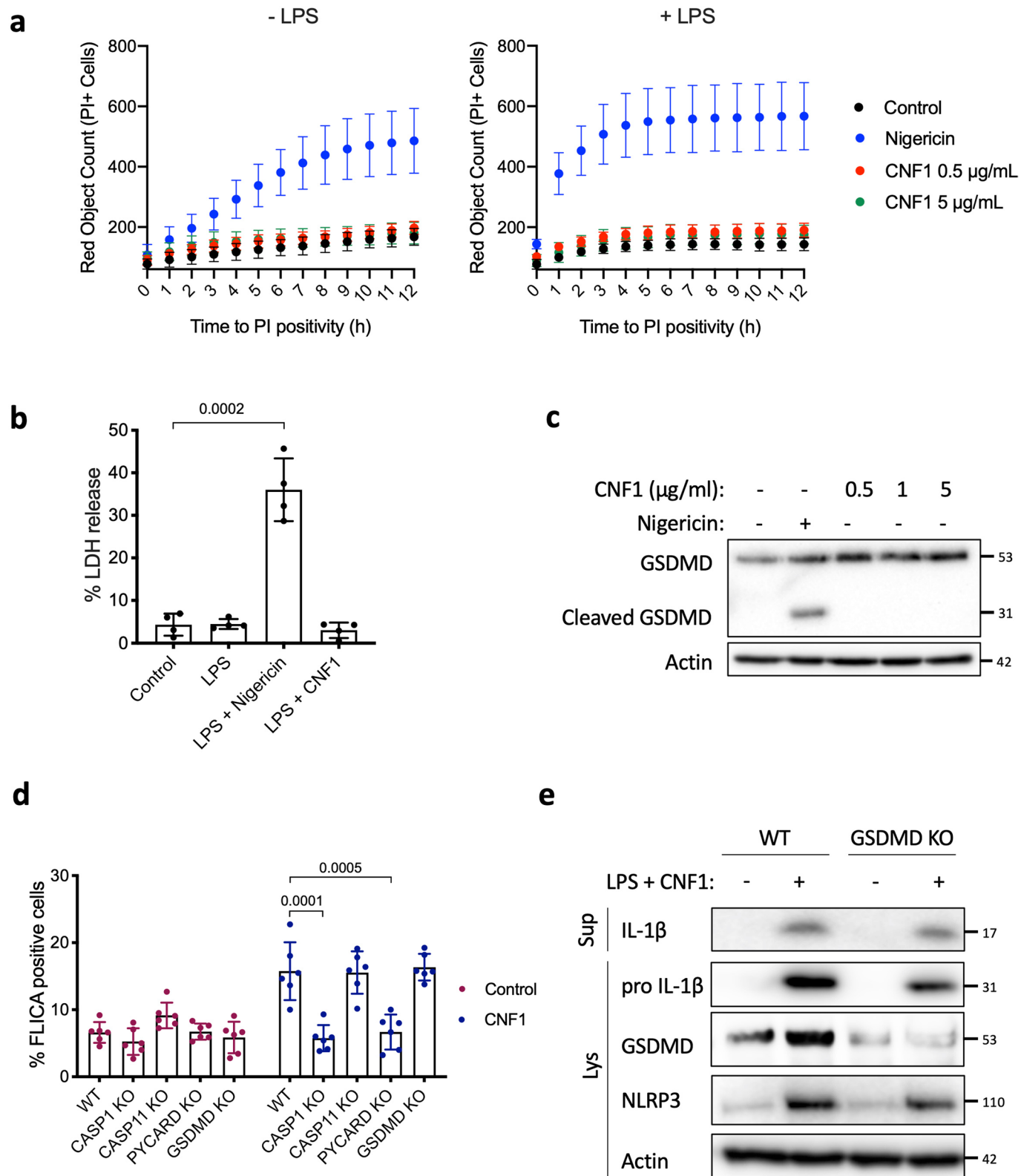
Publisher's note Springer Nature remains neutral with regard to jurisdictional claims in published maps and institutional affiliations.

© The Author(s), under exclusive licence to Springer Nature Limited 2021



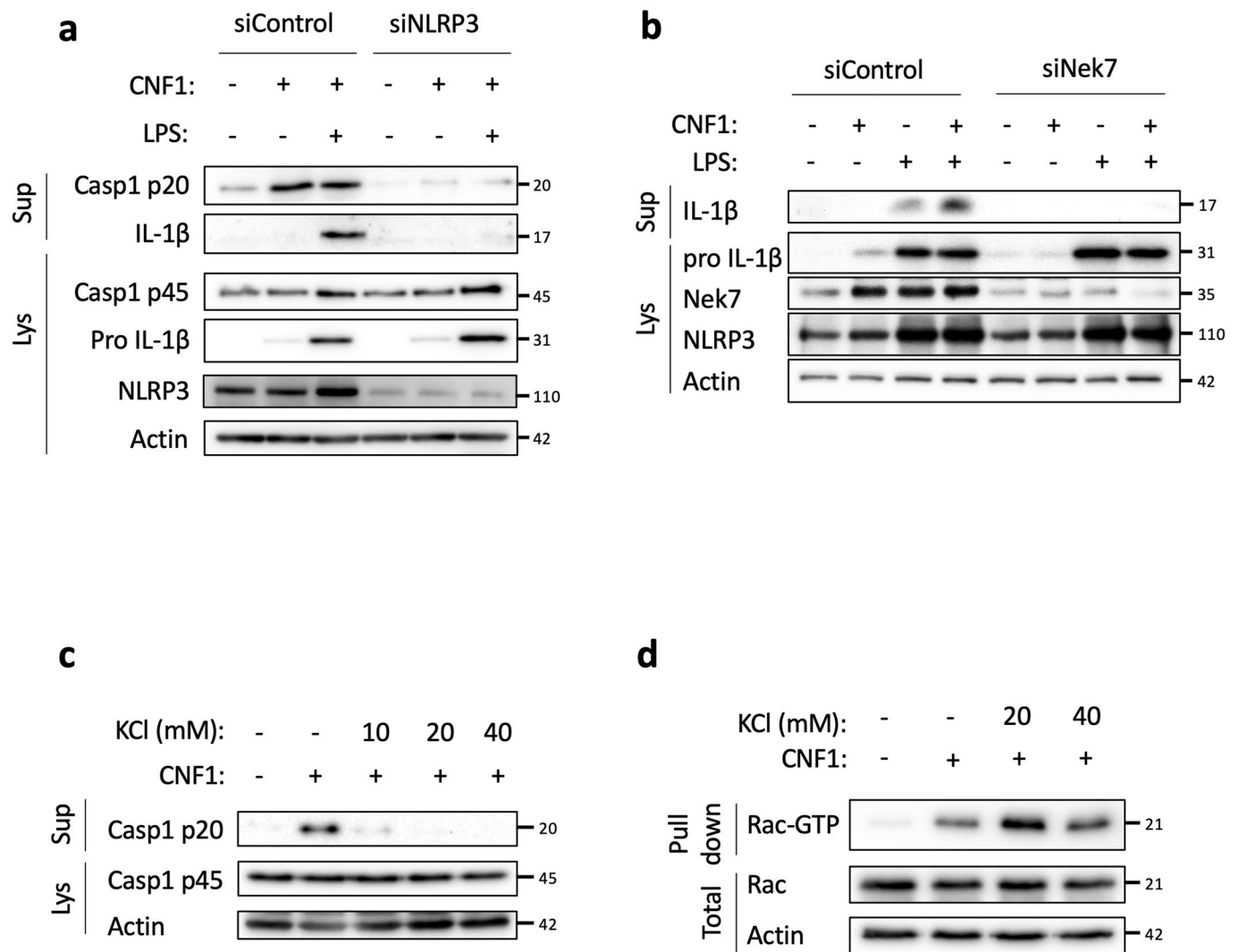
Extended Data Fig. 1 | See next page for caption.

Extended Data Fig. 1 | CNF1 triggers Caspase-1 activation and ASC specks formation. **a**, BMDMs isolated from BALB/c mice were either treated with vehicle (control) or CNF1 (500 ng ml⁻¹), inactive catalytic mutant CNF1 C866S (500 ng/mL) for 6 h, or Nigericin (5 μM) for 30 min. Active Caspase-1 was revealed with FAM-FLICA (green), ASC was stained using an anti-ASC antibody (Texas Red), nuclei and actin filament were stained with Hoechst and phalloidin-Alexa 647 respectively. Cells were analyzed by confocal microscopy. Arrows indicates FAM-FLICA dots that colocalize with the ASC staining. Scale bar: 10 μm. **b**, BMDM isolated from C57BL/6 J mice constitutively expressing ASC-citrine fusion protein (R26-CAG-ASC-citrine) were transfected with the indicated siRNA for 72 h prior to 6 h of CNF1 treatment (500 ng/mL) or treated with vehicle (control). Percent of cells with ASC specks. Data are expressed as the mean ± SEM. Each dot represents 10⁵ cells (n = 2 biologically independent samples). **c**, BMDM isolated from C57BL/6 J mice constitutively expressing ASC-citrine fusion protein (R26-CAG-ASC-citrine) were treated 6 h with CNF1 (500 ng/mL) or Nigericin (5 μM) for 30 min or vehicle (control). Cells were analyzed for ASC speck formation by flow cytometry as indicated, doublets were excluded using SSC-A and SSC-H plot, cells with a high expression of ASC-citrine were gated and then analyzed for ASC-citrine area (ASC-citrine-A) and ASC-citrine height (ASC-citrine-H). Cells with ASC specks are defined with a higher ASC-H:ASC-A ratio. Experiments were repeated at least three times, and representative data are shown.

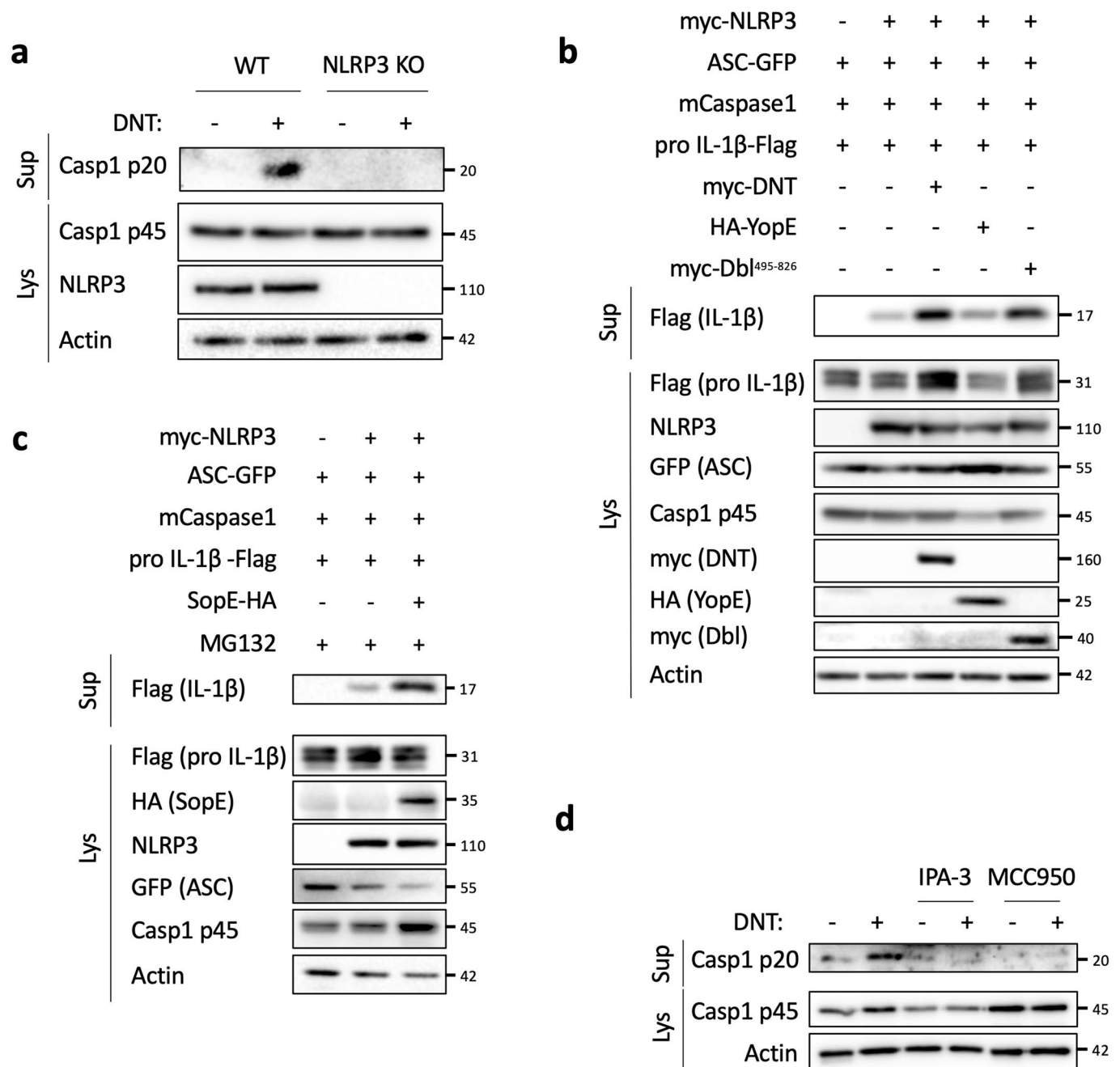


Extended Data Fig. 2 | See next page for caption.

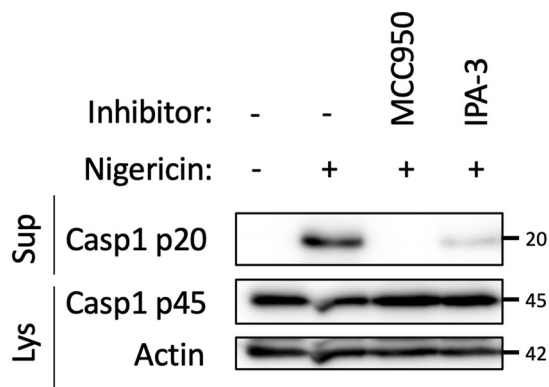
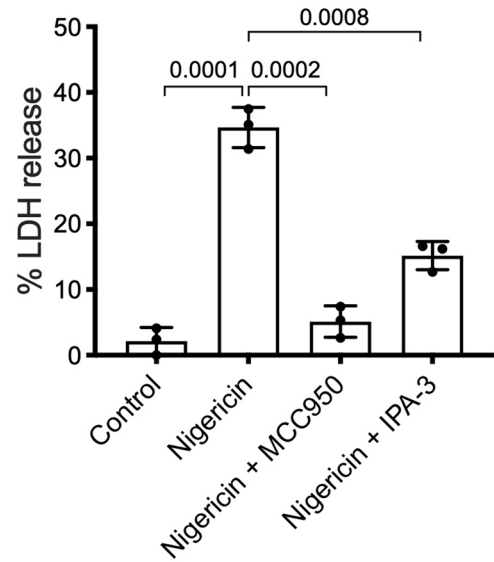
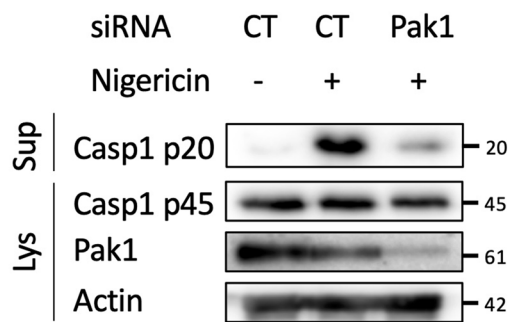
Extended Data Fig. 2 | NLRP3 inflammasome activation by CNF1 does not induce pyroptosis. **a**, BMDMs isolated from C57BL/6 J mice were treated with vehicle (control), Nigericin (5 μ M) or CNF1 (500 ng/mL or 5 μ g/mL) with or without LPS (100 ng/mL). Propidium iodide (PI) uptake was monitored over time (red object count) by real time imaging. Data are expressed as mean \pm SD. 10^4 cells were analyzed for each replicate (n = 4 independent wells). **b**, BMDMs isolated from C57BL/6 J mice were treated with vehicle (control, n = 6 independent experiments), LPS (100 ng/mL, n = 4 independent experiments), LPS and CNF1 (500 ng/mL, n = 6 independent experiments) or LPS and Nigericin (5 μ M, n = 4 independent experiments), and LDH release was assessed. Data are expressed as the mean \pm SEM. Statistical analyses were performed using a two-tailed nonparametric Mann Whitney test. **c**, BMDMs isolated from C57BL/6 J mice were treated either with Nigericin (5 μ M) for 30 min or CNF1 (0.5, 1 or 5 μ g/mL) for 8 h and GSDMD cleavage in cell lysates is shown. **d**, BMDMs isolated from C57BL/6 J wild-type or CASP1, CASP11, PYCARD (coding for ASC) or GSDMD knock-out mice were untreated or treated with CNF1 (500 ng/mL) for 6 h and were analyzed for Caspase-1 activation using the FAM-FLICA probe. Data are expressed as the mean \pm SEM. Statistical analyses were performed using a two-tailed unpaired Student's t-test. Each dot represents 100 cells (n = 700 cells). **e**, BMDMs isolated from wild-type or GSDMD knock-out mice were treated with CNF1 (500 ng/mL) and LPS (100 ng/mL) for 8 h as indicated. Supernatants and cell lysates were analyzed by immunoblot. The numbers on the side of the immunoblots indicate molecular weight (kDa). Experiments were repeated at least three times, and representative data are shown.



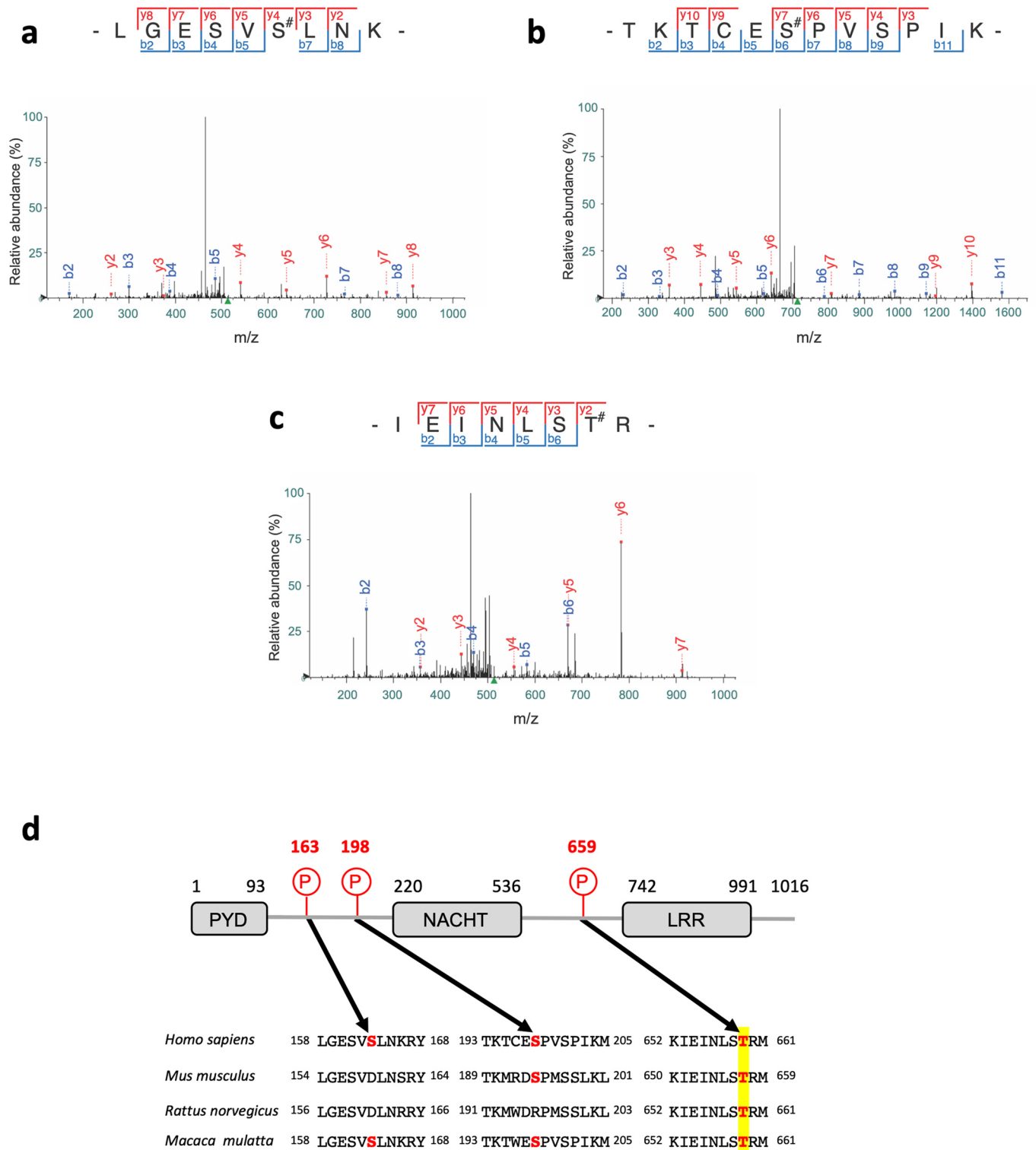
Extended Data Fig. 3 | CNF1-triggered inflammasome activation depends on NLRP3, Nek7 and K⁺ efflux. **a,b**, BMDMs isolated from C57BL/6J mice were transfected with siRNA-targeting NLRP3 (**a**), siRNA-targeting Nek7 (**b**), or control non-targeting siRNA for 72 h before treatment with CNF1 (500 ng/mL) and/or LPS (100 ng/mL) for 8 h. Supernatants and cell lysates were analyzed by immunoblot. **c,d**, BMDMs isolated from C57BL/6J mice (**c**) or iBMDMs (**d**) were treated with the indicated KCl concentration and CNF1 (500 ng/mL) for 8 h. **c**, Supernatants and cell lysates were analyzed by immunoblot, or (**d**) cell lysates were analyzed using a GST-Pak-RBD pull-down assay. The Rac associated with the GST-Pak-RBD beads is indicated as Rac-GTP. The numbers on the side of the immunoblots indicate molecular weight (kDa). Experiments were repeated at least three times, and representative data are shown.



Extended Data Fig. 4 | Toxins mediated Rho GTPases activation but not inhibition trigger the NLRP3 inflammasome. a, BMDMs isolated from wild-type or NLRP3 knock out C57BL/6J mice were treated with DNT (1 μ g/mL) for 8 h. Supernatants and cell lysates were analyzed by immunoblot. **b-c**, HEK293T cells were transfected as indicated with plasmids encoding NLRP3 inflammasome components (myc-NLRP3, ASC-GFP, mCaspase-1) and pro-IL-1 β -Flag together with **(b)** myc-DNT, HA-YopE or myc-DbI⁴⁹⁵⁻⁸²⁶ or **(c)** transfected with SopE-HA and treated with MG132 to block SopE degradation (10 μ M). Supernatants and cell lysates were analyzed by immunoblot. **d**, BMDMs isolated from C57BL/6J mice were treated with IPA-3 (5 μ M) or MCC950 (1 μ M) for 45 min prior to 8 h of DNT treatment (1 μ g/mL). Supernatants and cell lysates were analyzed by immunoblot. The numbers on the side of the immunoblots indicate molecular weight (kDa). Experiments were repeated at least three times, and representative data are shown.

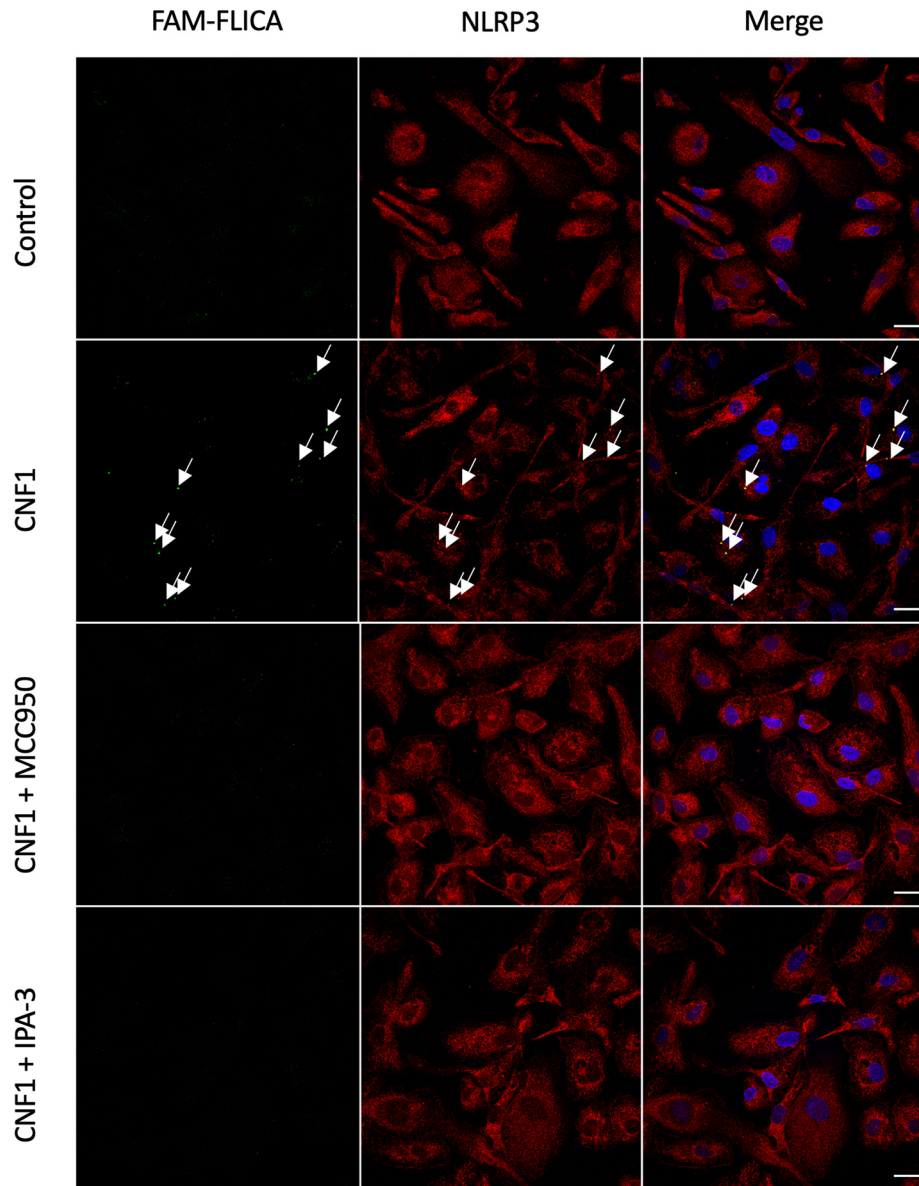
a**b****c**

Extended Data Fig. 5 | Inhibition of Pak1 diminishes NLRP3 activation by Nigericin. **a,b**, BMDMs isolated from C57BL/6 J mice were treated with MCC950 (1 μ M) or IPA-3 (5 μ M) for 45 min prior to Nigericin (5 μ M) treatment for 30 min. Supernatants and cell lysates were analyzed by **(a)** immunoblot and **(b)** supernatants were analyzed for LDH release ($n=3$ biologically independent experiments). Statistical analyses were performed using a two-tailed nonparametric Mann Whitney test. $n=3$ biologically independent samples were analyzed. **c**, BMDMs isolated from C57BL/6 J mice were treated for 72 h with non-targeting (CT) or Pak1-targeting siRNA before treatment with Nigericin (5 μ M) for 30 min. Supernatants and cell lysates were analyzed by immunoblot. The numbers on the side of the immunoblots indicate molecular weight (kDa). Experiments were repeated at least three times, and representative data are shown. Data are expressed as the mean \pm SEM.

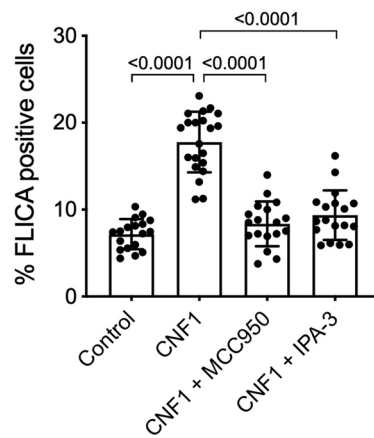


Extended Data Fig. 6 | Mass spectrometry analysis of Pak1 triggered NLRP3 phosphorylation. **a-c**, Fragmentation spectra of human NLRP3 peptides showing phosphorylation of Ser-163, Ser-198 and Thr-659. **d**, Representation of NLRP3 domain structure and sequence alignment of NLRP3 ortholog peptides surrounding phosphorylated residues identified by mass spectrometry. The phosphorylated residues are in bold red.

a

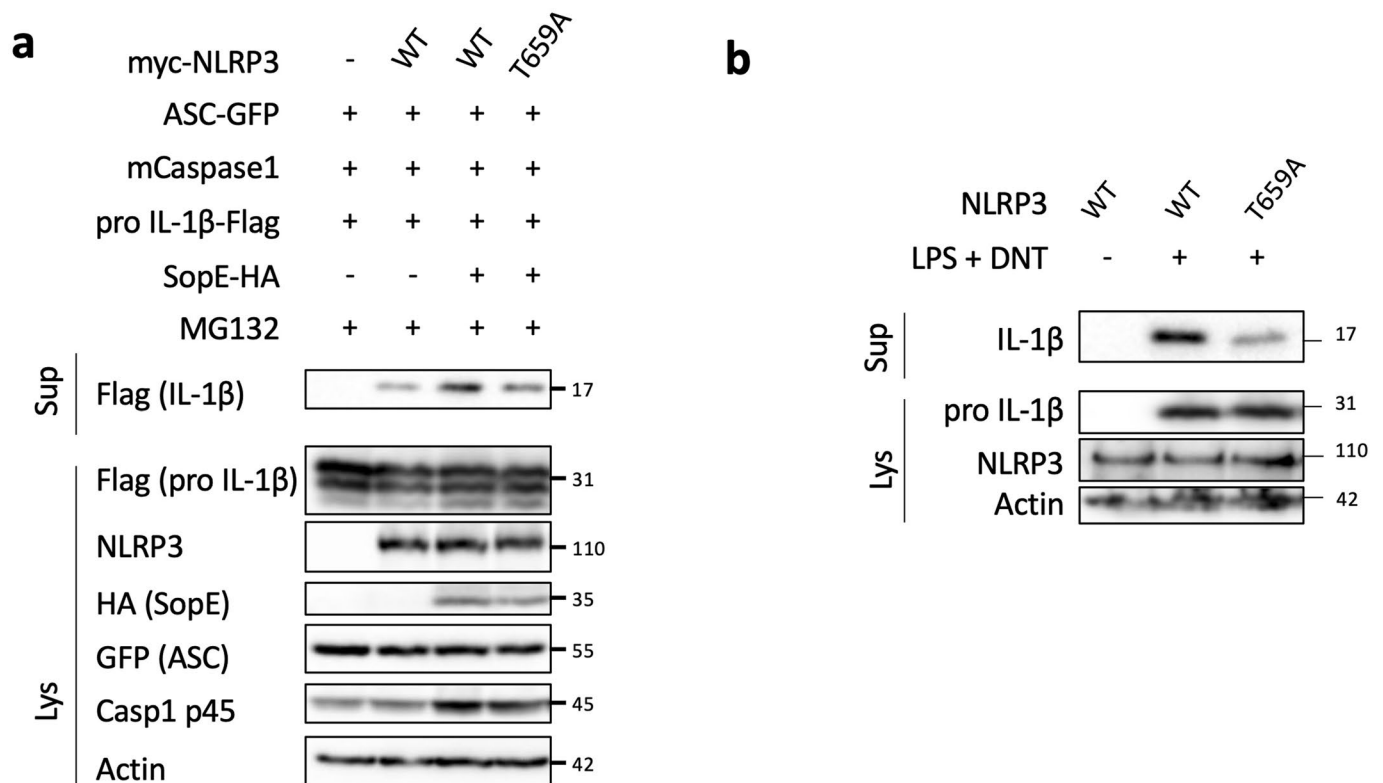


b



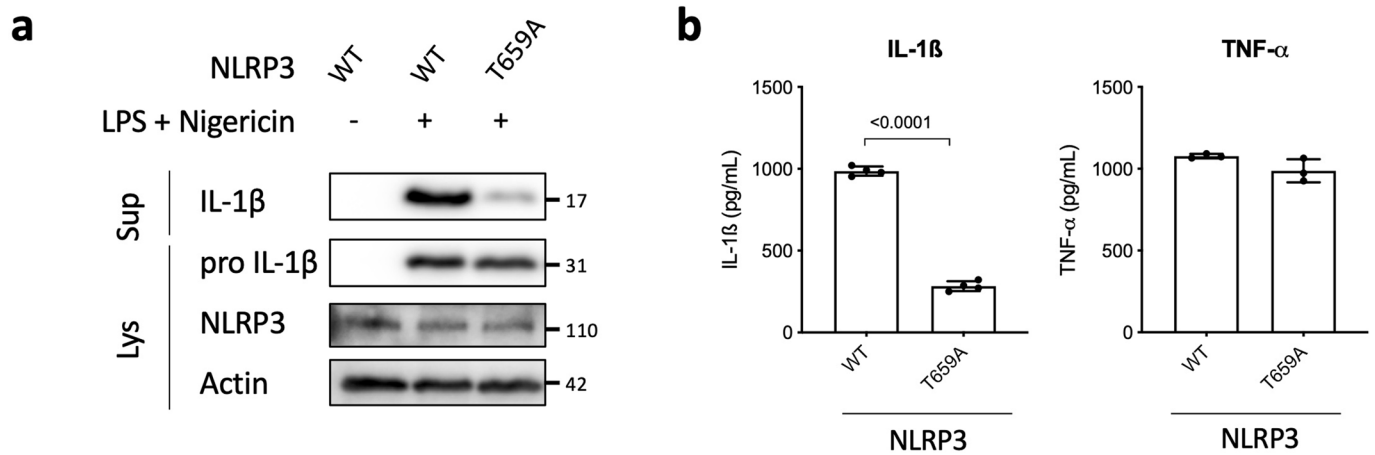
Extended Data Fig. 7 | See next page for caption.

Extended Data Fig. 7 | Conservation of the Pak-NLRP3 axis in Human monocyte-derived macrophages. a-b, Human monocyte-derived macrophages (hMDMs) were pretreated with vehicle, MCC950 (1 μ M) or IPA-3 (5 μ M) for 45 min before CNF1 (500 ng/mL) treatment for 6 h. Active Caspase-1 was stained with FAM-FLICA (green), NLRP3 (red) and nuclei (blue) were stained for immunofluorescence and confocal microscopy imaging. Arrows indicates FAM-FLICA dots that colocalize with NLRP3. Scale bar: 20 μ m. **b,** quantification of FAM-FLICA positive cells. Data are expressed as the mean \pm SEM. Statistical analyses were performed using a two-tailed unpaired Student's t-test. Each dot represents 100 cells (n = 1800 cells). Experiments were repeated at least three times, and representative data are shown.

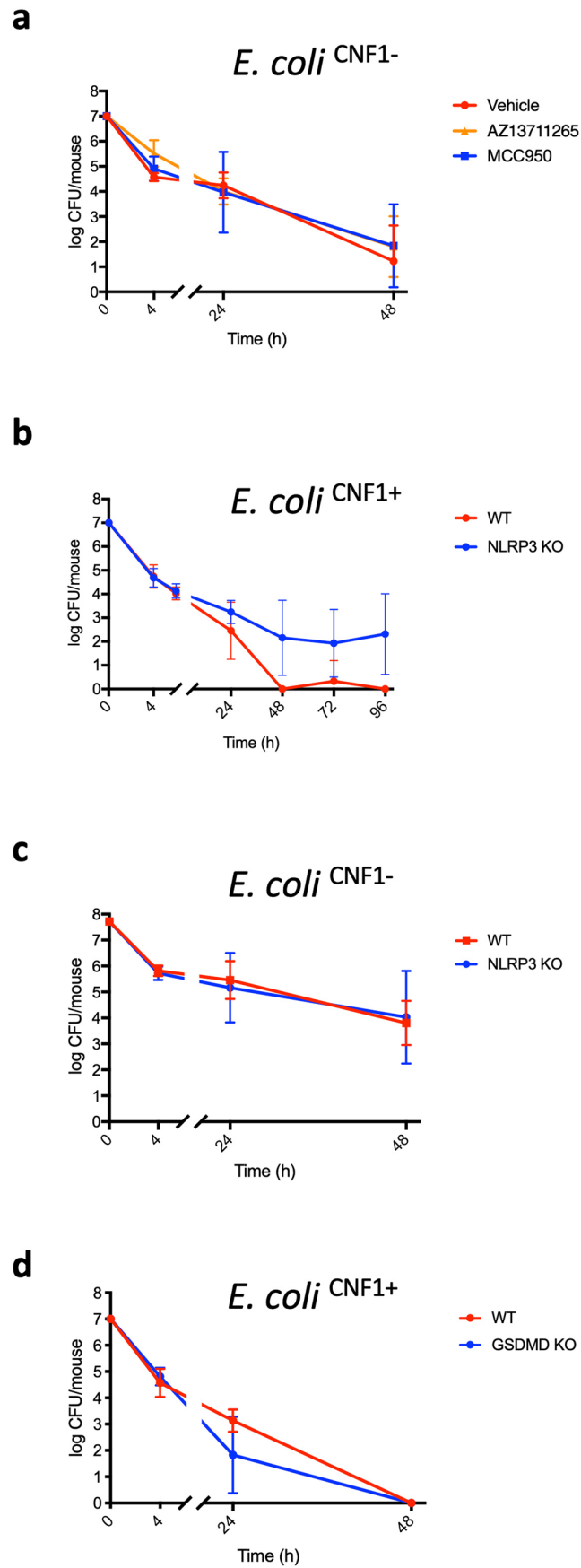


Extended Data Fig. 8 | The NLRP3 T659A mutant inhibit the IL-1 β maturation triggered by SopE and DNT. **a**, HEK293T cells were transfected with plasmids encoding NLRP3 inflammasome components (ASC-GFP, mCaspase-1) and pro-IL-1 β -Flag and either myc-NLRP3 (WT) or myc-NLRP3 T659A together with SopE-HA and treated with MG132 (10 μ M) to block SopE degradation. Supernatants and cell lysates were analyzed by immunoblot.

b, NLRP3 knock-out iBMDMs reconstituted either with NLRP3 or NLRP3 T659A were treated with vehicle or LPS (100 ng/mL) and DNT (1 μ g/mL) for 8 h. The numbers on the side of the immunoblots indicate molecular weight (kDa). Experiments were repeated at least three times, and representative data are shown.



Extended Data Fig. 9 | Macrophages expressing the NLRP3 T659A mutant have an impaired Nigericin- triggered IL-1 β maturation. a-b, iBMDMs stably expressing either NLRP3 or NLRP3 T659A were treated with Nigericin (5 μ M) for 30 min. Supernatants and cell lysates were analyzed by immunoblot and by ELISA for IL-1 β ($n = 4$ biologically independent samples) and TNF- α ($n = 3$ biologically independent samples). Data are expressed as the mean \pm SEM. Statistical analyses were performed using a two-tailed unpaired Student's t-test. The numbers on the side of the immunoblots indicate molecular weight (kDa). Experiments were repeated at least three times, and representative data are shown.



Extended Data Fig. 10 | See next page for caption.

Extended Data Fig. 10 | *E. coli*^{CNF1-} clearing is not affected by Pak1 or NLRP3 inhibition and *E. coli*^{CNF1+} clearing does not rely on GSDMD. a-d, Wild-type or knock-out mice were infected intravenously with isogenic CNF1-deleted *E. coli* (*E. coli*^{CNF1-}) or CNF1 expressing *E. coli* (*E. coli*^{CNF1+}). **a**, Wild-type mice were injected intraperitoneally with 10 mg/kg AZ13711265 or 50 mg/kg MCC950 or vehicle once a day and were infected intravenously with isogenic CNF1-deleted *E. coli* (*E. coli*^{CNF1-}) prior to the collection of peripheral blood at 4 h, 24 h and 48 h for measurement of bacteraemia (n = 5 mice per group). **b**, Wild-type or NLRP3 knock-out C57BL/6 J mice were infected intravenously with CNF1 expressing *E. coli* (*E. coli*^{CNF1+}) prior to the collection of peripheral blood at 4 h, 24 h, 48 h, 72 h and 96 h for measurement of bacteraemia (n = 6 per group). **c**, Wild-type (n = 6 mice) or NLRP3 knock-out C57BL/6 J mice (n = 4 mice) were infected intravenously with isogenic CNF1-deleted *E. coli* (*E. coli*^{CNF1-}) prior to the collection of peripheral blood at 4 h, 24 h and 48 h for measurement of bacteraemia (n = 6 per group). **d**, Wild-type (n = 6 mice) or GSDMD knock-out C57BL/6 J mice (n = 6 mice) were infected intravenously with *E. coli*^{CNF1+} prior to the collection of peripheral blood at 4 h, 24 h and 48 h for measurement of bacteraemia. Experiments were repeated two times and representative data are shown. Data are expressed as the geometric mean \pm 95 CI.

Reporting Summary

Nature Research wishes to improve the reproducibility of the work that we publish. This form provides structure for consistency and transparency in reporting. For further information on Nature Research policies, see [Authors & Referees](#) and the [Editorial Policy Checklist](#).

Statistics

For all statistical analyses, confirm that the following items are present in the figure legend, table legend, main text, or Methods section.

n/a Confirmed

- The exact sample size (n) for each experimental group/condition, given as a discrete number and unit of measurement
- A statement on whether measurements were taken from distinct samples or whether the same sample was measured repeatedly
- The statistical test(s) used AND whether they are one- or two-sided
Only common tests should be described solely by name; describe more complex techniques in the Methods section.
- A description of all covariates tested
- A description of any assumptions or corrections, such as tests of normality and adjustment for multiple comparisons
- A full description of the statistical parameters including central tendency (e.g. means) or other basic estimates (e.g. regression coefficient) AND variation (e.g. standard deviation) or associated estimates of uncertainty (e.g. confidence intervals)
- For null hypothesis testing, the test statistic (e.g. F , t , r) with confidence intervals, effect sizes, degrees of freedom and P value noted
Give P values as exact values whenever suitable.
- For Bayesian analysis, information on the choice of priors and Markov chain Monte Carlo settings
- For hierarchical and complex designs, identification of the appropriate level for tests and full reporting of outcomes
- Estimates of effect sizes (e.g. Cohen's d , Pearson's r), indicating how they were calculated

Our web collection on [statistics for biologists](#) contains articles on many of the points above.

Software and code

Policy information about [availability of computer code](#)

Data collection

Data analysis

For manuscripts utilizing custom algorithms or software that are central to the research but not yet described in published literature, software must be made available to editors/reviewers. We strongly encourage code deposition in a community repository (e.g. GitHub). See the Nature Research [guidelines for submitting code & software](#) for further information.

Data

Policy information about [availability of data](#)

All manuscripts must include a [data availability statement](#). This statement should provide the following information, where applicable:

- Accession codes, unique identifiers, or web links for publicly available datasets
- A list of figures that have associated raw data
- A description of any restrictions on data availability

All data supporting the findings of this study are available within the article and its supplementary information or from the corresponding author upon reasonable request. Source data are provided with this paper.

Field-specific reporting

Please select the one below that is the best fit for your research. If you are not sure, read the appropriate sections before making your selection.

- Life sciences Behavioural & social sciences Ecological, evolutionary & environmental sciences

Life sciences study design

All studies must disclose on these points even when the disclosure is negative.

| | |
|-----------------|--|
| Sample size | For experiments involving quantification, n=3 was chosen as the minimal replicate number, and sample size was determined by the number positive cells or samples within the replicates. We determined this to be sufficient owing to internal control (specific staining of known markers) and low observed variability between samples. For mice experiments, calculations were based on previous publication (Diabaté et al 2015; DOI: 10.1371/journal.ppat.1004732) and the G*Power software. |
| Data exclusions | No data were excluded |
| Replication | For all the data presented attempts were successful. The patterns of marker observed were consistent between experiments and with previously known results. Experiments were repeated at least three times and performed independently. |
| Randomization | Field used for imaging were selected randomly by the microscope. All cells and puncta that passed quality control were analyzed equally. |
| Blinding | Investigators were blinded for in vivo experiments and RNAi screen experiments. For other experiments, the investigators were blinded to group allocation during data collection. |

Reporting for specific materials, systems and methods

We require information from authors about some types of materials, experimental systems and methods used in many studies. Here, indicate whether each material, system or method listed is relevant to your study. If you are not sure if a list item applies to your research, read the appropriate section before selecting a response.

Materials & experimental systems

| n/a | Involved in the study |
|-------------------------------------|---|
| <input type="checkbox"/> | <input checked="" type="checkbox"/> Antibodies |
| <input type="checkbox"/> | <input checked="" type="checkbox"/> Eukaryotic cell lines |
| <input checked="" type="checkbox"/> | <input type="checkbox"/> Palaeontology |
| <input type="checkbox"/> | <input checked="" type="checkbox"/> Animals and other organisms |
| <input checked="" type="checkbox"/> | <input type="checkbox"/> Human research participants |
| <input checked="" type="checkbox"/> | <input type="checkbox"/> Clinical data |

Methods

| n/a | Involved in the study |
|-------------------------------------|--|
| <input checked="" type="checkbox"/> | <input type="checkbox"/> ChIP-seq |
| <input type="checkbox"/> | <input checked="" type="checkbox"/> Flow cytometry |
| <input checked="" type="checkbox"/> | <input type="checkbox"/> MRI-based neuroimaging |

Antibodies

| | |
|-----------------|---|
| Antibodies used | <p>rabbit anti-ASC (AG-25B-0006, Adipogen) rabbit anti-Phospho-Pak (ab40795, Abcam) TexasRed anti-mouse IgG (TI-2000, Vector Laboratories) Cy5 anti-mouse IgG (715-175-151, Jackson ImmunoResearch) TexasRed anti-rabbit IgG (711-075-152, Jackson ImmunoResearch) rabbit anti-IL-1β (GTX74034, Genetex) mouse anti-Caspase-1 (clone Casper-1, Adipogen) mouse anti-Rac (clone 102/Rac1, BD Biosciences) goat anti-Rac2 (ab2244, Abcam) mouse anti-NLRP3 (clone Cryo-2, Adipogen) rabbit anti-Nek7 (ab133514, Abcam) rabbit anti-Pak1 (2602, CST) rabbit anti-Pak2 (2608, CST) mouse anti-β-actin (AC-74, Sigma) mouse anti-Myc (9E10, Roche) mouse anti-HA (16B12, Covance) mouse anti-Flag (clone M2, Sigma) mouse anti-GFP (clone 7.1, 13.1, Roche) rabbit anti-GSDMD (ab209845)</p> |
| Validation | <p>Antibodies were all validated by the manufacturer. Primary antibodies directed against ASC, Pak1, Pak2, Caspase-1, Rac, Rac2, NLRP3, Nek7, GSDMD were validated in this study or in our previous publication (Diabaté et al 2015; DOI: 10.1371/journal.ppat.1004732) by western-blot using either cells lysated collected from transfected by the corresponding siRNA or from the corresponding knock-out macrophages.</p> |

Eukaryotic cell lines

Policy information about [cell lines](#)

| | |
|--|--|
| Cell line source(s) | HEK293T, Immortalized BMDM |
| Authentication | All cell lines were authenticated by using PCR with species specific primers |
| Mycoplasma contamination | Cells were tested negative for mycoplasma contamination |
| Commonly misidentified lines (See ICLAC register) | No commonly misidentified cell lines were used. |

Animals and other organisms

Policy information about [studies involving animals](#); [ARRIVE guidelines](#) recommended for reporting animal research

| | |
|-------------------------|---|
| Laboratory animals | <p>BALB/c mice C57BL/6J mice C57BL/6J NLRP3 KO mice C57BL/6J Pak1 KO mice C57BL/6J GSDMD KO mice C57BL/6J ASC-citrine mice</p> <p>7 weeks-old mice were housed with their littermates and kept on a regular 12-h light/dark cycle, room temperature: 20–25 °C; relative humidity: 50–70%. Food and water were available ad libitum.</p> |
| Wild animals | the study did not involved wild animals |
| Field-collected samples | the study did not involved sample collected from the field |
| Ethics oversight | This study was carried out in strict accordance with the guidelines of the Council of the European Union (Directive 86/609/EEC) regarding the protection of animals used for experimental and other scientific purposes. The protocol was approved by the Institutional Animal Care and Use Committee on the Ethics of Animal Experiments of Nice, France (reference: APAFIS#18322-20181218099427035 v2). |

Note that full information on the approval of the study protocol must also be provided in the manuscript.

Flow Cytometry

Plots

Confirm that:

- The axis labels state the marker and fluorochrome used (e.g. CD4-FITC).
- The axis scales are clearly visible. Include numbers along axes only for bottom left plot of group (a 'group' is an analysis of identical markers).
- All plots are contour plots with outliers or pseudocolor plots.
- A numerical value for number of cells or percentage (with statistics) is provided.

Methodology

| | |
|---------------------------|--|
| Sample preparation | BMDM isolated from C57BL/6J mice constitutively expressing ASC-citrine fusion protein (R26-CAG-ASC-citrine) were treated with LPS (100 ng/mL) for 16h before 6h of treatment with vehicle or CNF1 (500 ng/mL) or 30 min with Nigericin (5µM). Cells were collected and analyzed by flow cytometry. |
| Instrument | Flow cytometry data were collected using the the BD FACSCanto II |
| Software | Flow cytometry data were analyzed using FlowJo v10.6.2 |
| Cell population abundance | For each sample, at least 10 000 ASC-citrine expressing cells were analyzed |
| Gating strategy | Doublets were excluded using SSC-A (area) and SSC-H (height) plot, cells with a high expression of ASC-citrine were gated and then analyzed for ASC-citrine signal area (ASC-citrine-A) and ASC-citrine signal height (ASC-citrine-H). Cells with ASC specks were defined with a higher ASC-H:ASC-A ratio. |

- Tick this box to confirm that a figure exemplifying the gating strategy is provided in the Supplementary Information.